TISSUE ENGINEERING APPROACHES FOR THE TREATMENT OF KNEE JOINT DAMAGE

A Dissertation

by

REBECCA ERIN MCMAHON

Submitted to the Office of Graduate Studies of
Texas A&M University
in partial fulfillment of the requirements for the degree of

DOCTOR OF PHILOSOPHY

May 2011

Major Subject: Chemical Engineering

Tissue Engineering Approaches for the Treatment of Knee Joint Damage

TISSUE ENGINEERING APPROACHES FOR THE TREATMENT OF KNEE JOINT DAMAGE

A Dissertation

by

REBECCA ERIN MCMAHON

Submitted to the Office of Graduate Studies of
Texas A&M University
in partial fulfillment of the requirements for the degree of

DOCTOR OF PHILOSOPHY

Approved by:

Co-Chairs of Committee,	Mariah Hahn
	Michael Pishko
Committee Members,	Arul Jayaraman
	Ibrahim Karaman
Head of Department,	Michael Pishko

May 2011

Major Subject: Chemical Engineering

ABSTRACT

Tissue Engineering Approaches for the
Treatment of Knee Joint Damage. (May 2011)
Rebecca Erin McMahon, B.S., Rensselaer Polytechnic Institute
Co-Chairs of Advisory Committee: Dr. Mariah Hahn
Dr. Michael Pishko

There are more than 150,000 anterior cruciate ligament reconstructions each year with the goal of recovering the balance between knee stability and mobility. As many as 25% of these procedures will end in joint instability that can cause further damage. The risk of developing degenerative joint disease (DJD) increases in patients with previous knee injury, resulting in a higher instance of total knee arthroplasty (TKA).

There are more than 400,000 TKA procedures each year, but the waiting lists for this surgery shows that many more patients are hoping to undergo this procedure. TKA provides improved knee function and pain relief for patients suffering from DJD. Although this procedure is considered successful, as younger patients undergo this treatment, the long-term performance must be improved. Major mechanisms of failure include component loosening from stress-shielding, poor integration of the implant with native tissue, and ion release from the implant. TiNb alloys are more biocompatible than currently used alloys, such as NiTi, and have mechanical properties closer to bone, so they would reduce the instance of stress shielding. TiNb can be made porous for better integration with the native bone and has superior corrosion resistance than NiTi.

Engineered ligaments have generally failed to achieve mechanical properties sufficiently similar to their native counterparts, but also lack the osteochondral interface critical to the transfer of load between ligament and bone. The osteochondral interface could be incorporated through a gradient of inorganic content toward the bony insertion ends of the ligament graft, as we showed that in increase of inorganic content resulted in

the transdifferentiation of osteoblasts toward chondrocyte-like cells (bone to cartilage-like).

A composite scaffold composed of an electrospun mesh with either a hydrogel component or extracellular matrix (ECM) produced by the cells may be a suitable tissue engineered ligament graft. The non-linear stress-strain behavior seen in native ligament is exhibited by both of these systems, and the ECM produced by these systems is consistent with ligament tissue. The ECM-electrospun mesh composite exhibited higher elastic modulus than the fibrin-electrospun mesh composite, but required extensive pre culture while the fibrin-electrospun mesh composite could be fabricated *in situ.*

ACKNOWLEDGEMENTS

I would like to thank my committee co- chairs, Dr. Mariah Hahn and Dr. Pishko, as well as my committee members, Dr. Jayaraman and Dr. Karaman for their guidance and support throughout the course of my research. Thanks also go to my group members, especially Dany Munoz-Pinto, Xin Qu, and Carolina Jimenez. My colleagues, collaborators, and the department faculty and staff made my time at Texas A&M University a great experience. Also, my gratitude extends to Dr. James and Dr. Taylor for their expertise and assistance in the ICP-MS measurements. Ann Ellis, Dr. Pendleton, and Dr. Holtzenburg were vital in developing my understanding of SEM sample preparation and imaging.

Finally, thanks to my family for their encouragement, and friends for their love and support. I could not have succeeded in this goal without the assistance and support from each of you.

TABLE OF CONTENTS

CHAPTER Page

LIST OF FIGURES

Page

LIST OF TABLES

CHAPTER I
INTRODUCTION

The number of patients on organ transplant lists far exceeds the number of organs available for transplant. These numbers do not account for patients with tissue damage such as burn victims, patients with critical sized bone defects, vascular disease, or any number of other conditions, which would benefit from tissue replacement. At present, physicians generally treat organ or tissue loss by transplanting organs from one individual to another, by performing reconstructive surgeries, or by using mechanical devices such as kidney dialyzers. Tissue engineering emerged from this shortfall in available tissue or organs and from issues surrounding long term use of external mechanical devices. The knee is the most injured joint and requires 400,000 total knee replacements per year.[1] Many of these come from patients with previous knee damage, like ligament ruptures, but many more come from sufferers of degenerative joint disease. Over 150,000 anterior cruciate ligament (ACL) reconstruction surgeries are performed each year due to damage or rupture of ligaments causing instability in the knee joint,[2] which can cause further knee damage if left untreated.[3-5] Tissue engineering could potentially provide improved ligament grafts to reduce the progressive degeneration of joints following injury. Tissue engineering principles could also be applied to improve the long-term success of total knee replacements. An understanding of the knee anatomy may provide the information necessary to improve the lives of patients with debilitating pain and low quality of life.

1.1 Native Knee Anatomy

An understanding of the normal anatomy of the knee, one of the most injured

---

This dissertation follows the style of *Journal of Biomedical Materials Research Part A.*

joints (shown in **Figure 1**), provides the insight for the design of tissue engineered approaches for the treatment of knee joint damage. The bones of the knee, the femur and the tibia, meet to form a hinge joint. Both of these bones are covered by a layer of cartilage that cushions the bones. The meniscus is a pad of cartilage that acts as a shock absorber to further cushion the joint. Damage to cartilage in the knee due to osteoarthritis or injury is the primary cause of knee pain.[6] The collateral ligaments run along the sides of the knee to limit sideways motion and the cruciate ligaments cross in the center of the knee. The anterior cruciate ligament (ACL) limits rotation and forward motion of the tibia, while the posterior cruciate ligament limits backward motion of the tibia. Knee injuries can span a range from injuries of the ligament alone to total joint damage. Each of these requires different treatment approaches.

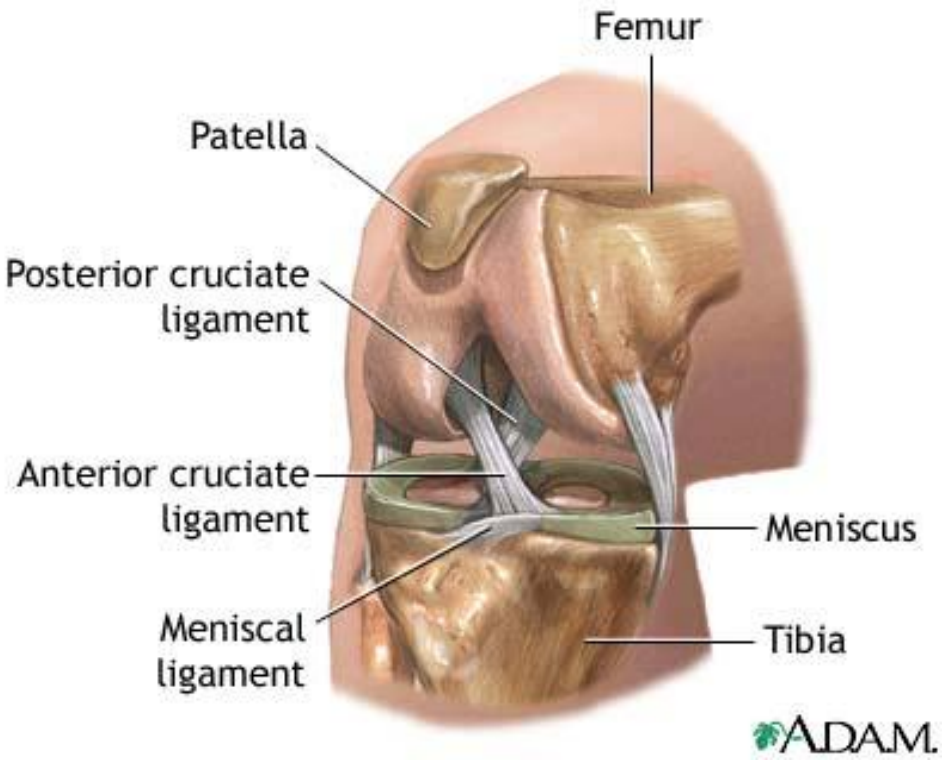

Figure 1: Anatomy of a healthy knee [7]

1.2 Current Treatments

The treatment for knee joint damage depends on the extent of injury or damage. The ACL is the most commonly injured ligament in the knee, yet this tissue has limited ability to heal. The incidence of knee ligament injuries have been estimated to be as many as 2 people in 1000 per year in the general population[8] and much higher in those involved in sports.[9] Ligament rupture can upset the balance between knee stability and mobility. Left untreated, this injury can result in damage to other parts of the joint leading to pain and morbidity, so surgery is the typical treatment. Ligament reconstruction surgery limits the potential for long-term knee instability, further damage to other parts of the knee, or progressive degeneration,[3-5] by restoring tibiofemoral stability, which can minimize the risk of further damage to the knee.[10,11] The ligament reconstruction procedure includes removing and replacing the existing tendon with either the central third of the patellar ligament or the hamstring tendons with fairly similar outcomes.[12-16] Bone tunnels are drilled into the tibial and femoral heads and the tendon or ligament is attached inside the tunnel using a metal or degradable PLLA screw.[17,18] There are more that 150,000 ligament reconstruction surgeries per year,[2] and while the majority of these procedures yield good short term results, up to 25% of patients experience complication including instability that can damage other knee structures.[19-23] An increased risk of developing degenerative joint disease exists after severe injury such as rupture of the ACL,[20,21] but even after a successful reconstructive surgery, loss of graft tension of failure of graft fixation can cause increased knee instability.[24,25] This instability along with articular cartilage and meniscal damage associated with ACL injury or rupture may be the cause of osteoarthritis later in life in many of these patients.

Several authors describe an increased danger of degenerative joint disease after a severe injury such as a traumatic rupture of the ACL,[20,21] which, in turn, increases the need for these patients to undergo total knee arthroplasty (TKA). With extensive knee damage due to disease or progressive degeneration following injury, TKA is often

performed as it provides improved knee function and pain relief. Currently there are over 380,000 TKA procedures in the US each year-- some to those with complications of ligament reconstructions, but many more from sufferers of degenerative disease-- but the waiting lists for this surgery show that many more patients are hoping to undergo this procedure. Without alternative treatments for degenerative knee disease, it is projected that by 2030, 3.4 million patients will undergo total knee replacements each year. This procedure involves removing the distal end of the femur and the proximal end of the tibia, then replacing the knee joint with a metal and plastic implant. Although 94-98% of TKA are still functional after 10-14 years,[26,27] there are a number of problems associated with this procedure, and with younger patients undergoing this surgery, the long-term performance of this implant is of increased importance.

Despite the advances in TKA technology, the major mechanisms of failure include polyethylene wear and component loosening.[23] There are many mechanisms of loosening, including stress shielding[28] which is caused by a mismatch between the mechanical properties of the implant and the native bone, ion leaching from the implant,[29] and poor ingrowth of bone into the implant. My project looks to use tissue engineering (TE) to improve the prospects for patients with less severe injuries, like ligament damage, but also for patients with extensive damage that requires TKA.

It is important to note the work in cartilage tissue engineering, whose progress may one day reduce the need for TKA procedures. Transplantation of chondrocytes or differentiated cells have been studied with a success rate of less than 40% due to the problem of retaining the cells in the defect for the length of time required to produce matrix.[30,31] Another study implanted autologous chondrocytes below a periosteal flap with better results over 5-10 years, but requires the harvest of periosteal tissue.[32] Cells encapsulated within a scaffold have also been investigated as a treatment for joint pain due to cartilage damage. The biomaterial can generally be injected to fill any shape or size defect then polymerized.[33,34] Although, cartilage tissue engineering doesn't treat the problem of degenerative joint disease, if used to treat injuries fairly soon after the

damage, perhaps this will delay the onset of or reduce the instance of degenerative joint disease, which may reduce the instance of TKA.

The understanding of materials and biology makes tissue engineering a discipline that has the potential to improve both ligament reconstruction surgeries and knee replacements.

1.3 Tissue Engineering

The modern era of TE began only about 25 years ago. In 1993, Langer and Vacanti defined TE as an interdisciplinary field that applies the principle of engineering and the life sciences toward the development of biological substitutes that restore, maintain, or improve tissue function.[35] The initial focus of this discipline involved *in vitro* creation of replacement tissues for simple tissues, like skin. The interest in designing more complex tissues than partial-thickness skin substitutes made it clear that the direct assembly of different cell types would be inadequate to recreate the structure and function of complex tissues. The basic principle of present TE is the combination of appropriate cells with biomaterials under conditions that promote and lead to tissue formation. In general, there are three strategies used to treat diseased or injured tissues. Cells from the patient or a donor can be implanted into the defect, either directly, or after being combined with a scaffold material. Alternatively, patient or donor cells can be grown on a scaffold to create a 3D tissue in vitro and then implanted after the construct has reached maturity. Finally, a scaffold material alone can be implanted directly and this material can stimulate the surrounding cells to promote local tissue repair.[36]

The assembly of cells into tissues is a complicated process where cells take cues from their microenvironmental niche. Each tissue provides a unique microenvironment with varying conditions such as: oxygen concentration, pH, available nutrients, mechanical forces, cytokine gradients, and ionic and electric potential. The complexity of the mature tissue development process can currently be aided with bioreactors, but the effect is limited. Implanting constructs into the body may aid in this development, but

the appropriate choice of cells and scaffold could determine the success or failure of this approach. Ideally, the scaffold would degrade at a similar rate as extracellular matrix (ECM) deposition so that eventually only the generated tissue would remain.

Tissue engineering and regenerative medicine present a possible solution to many common knee problems and potential improvements to current treatments. Less stiff and more biologically inert metal alloys such as Ti alloys have been applied with success and excellent bone ingrowth into porous materials. Tissue engineered ligament grafts may be applied without the common problems associated with currently used grafts such as autografts, which can cause pain and donor site morbidity.

1.4 Cell Source

Cell source became a limitation for the design and commercial application of tissue engineered constructs as the first tissue engineered constructs either relied on migration of host cells into scaffolds, with limited success, or used adult cells in the design of constructs.[37] Mature autologous cells are a good option for tissue engineered constructs, but may not always be available, viable, or capable of the proliferation necessary for forming new tissue.

With the discovery and better understanding of adult and embryonic stem cell biology, and more recently induced pluripotent stem cells, cell source became less of a problem in tissue engineering. Mesenchymal stem cells have the ability to differentiate into many mesenchymal cell types, like bone, cartilage, fat, dermis, muscle, bone marrow stroma, and ligament/tendon, making them a good candidate for ligament tissue engineering. Many researchers are interested in bone marrow derived mesenchymal stem cells as stem cells for many tissues.[38]

The ability to heal following injury is reduced as humans age. This can be explained by the decline in the number of MSCs in the bone marrow.(Shown in **Figure 2**) Knee injury often occurs in adults, with very low MSCs per bone marrow cells, so these cells may not be the best option for ligament tissue engineering applications.

Adipose tissue is fairly simple to extract and contains high levels of MSCs.[39] These cells are thought to be associated with the blood vessels within these tissues.[40] Adipose derived MSCs could potentially be a viable option for treatment of knee joint damage due to their mesenchymal differentiation potential and the abundance in adipose tissue.

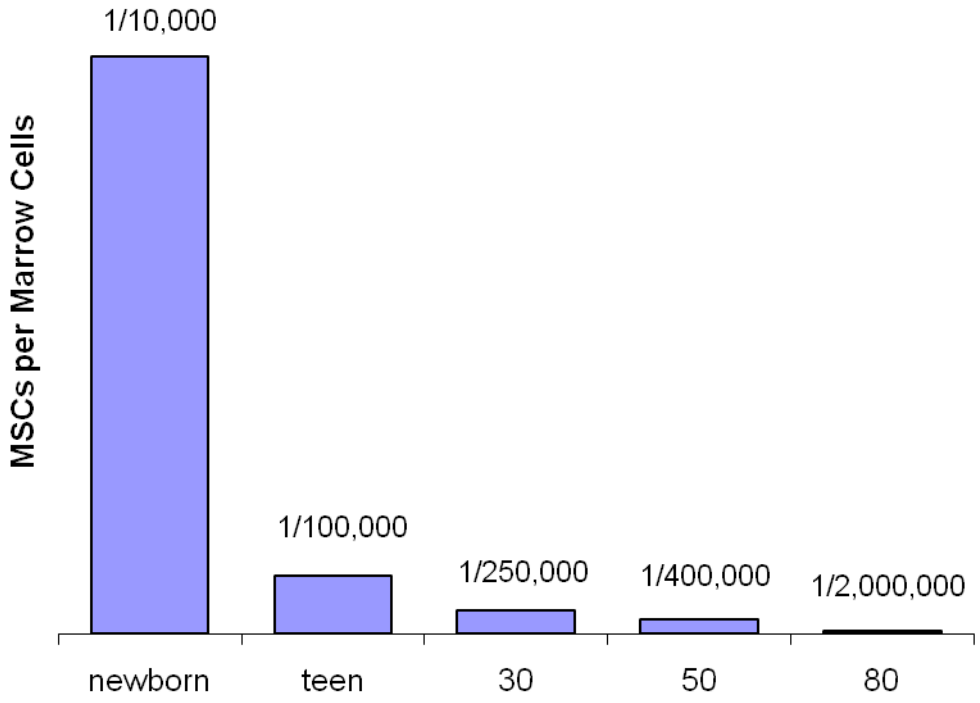

Figure 2 : Human MSC Decline with Age (Adapted from Caplan) [41]

1.5 Biomaterial Choice

A tissue engineering scaffold is a material that supports the cells for their growth, proliferation, and differentiation in the absence of native ECM. For bone applications, like in total joint replacements, metals act as a scaffold and should be porous to promote

bone ingrowth, which can secure the implant to reduce loosening. For soft tissues, such as ligament, the mechanical properties of polymers more closely match native tissues.

The ECM was originally thought to act only as a mechanical support for the cells, but through receptors on the surface of cells, the ECM takes part in promoting cell adhesion, migration, growth, differentiation, and apoptosis.[42] Ideally, a tissue engineered scaffold should mimic both the form and function of native ECM. Like any other biomaterial for implantation, a tissue engineered scaffold should be biocompatible and not initiate tissue reactions or immune responses. For most applications, the scaffold should be biodegradable at a rate that allows cells to produce ECM to fill the void left from the degrading scaffold. With proper scaffold selection, there will be no fibrous encapsulation of the materials and the newly formed tissue with integrate with the surrounding tissue in a way that leaves no residual evidence of implantation.[43]

Current biodegradable materials do not provide the necessary mechanical properties for joint replacement applications, so metals are used fairly successfully. Metal processing and coatings can produce porous scaffolds that promote bone ingrowth and cell differentiation.

1.6 Experimental Plan

My research focuses on applying tissue engineering principles to better the design of tissue engineering scaffolds for treating both ligament damage alone and total knee replacements. The overall approach to this work is outlined in **Figure 3**.

In terms of total knee replacement, my work focuses on the metallic component and exploring alternatives to Nitinol (NiTi) alloys. The first objective of my work was therefore to determine the biocompatibility and corrosion resistance of a TiNb shape memory alloy (SMA) in physiological conditions. This material has properties that could be exploited for bone tissue engineering, vascular stents, and medical and dental wires. It could potentially replace NiTi, which has controversial biocompatibility, for most applications.

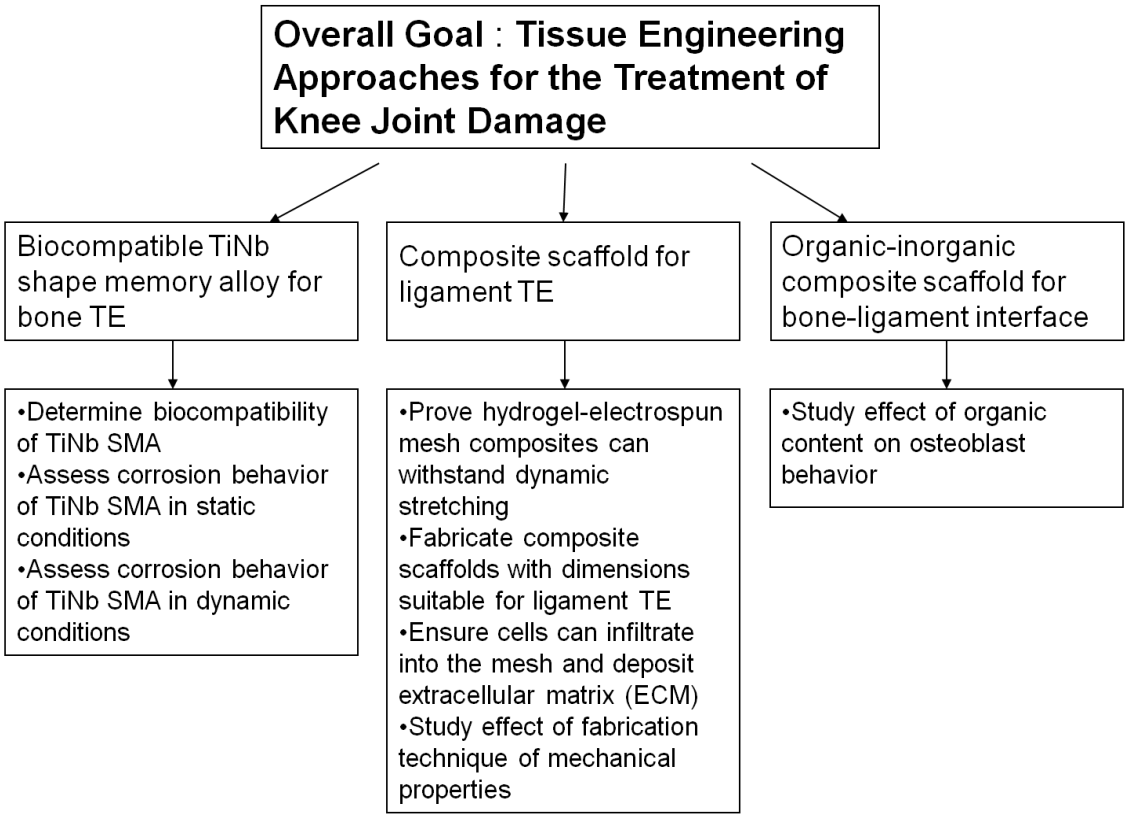

Figure 3 : Scope of research

In terms of ligament tissue engineering, electrospun mesh is an attractive scaffold for ligament tissue engineering because of the high tensile strength and aligned fibers which are suitable for the regeneration of oriented tissues, like ligament. Fabrication of electrospun meshes with dimension suitable for clinical application (e.g. 30 mm length by 7 mm in diameter for adult human ACL) is difficult as the generation of structures with thicknesses of 1 mm or greater is very time intensive. Therefore, a composite scaffold composed of the electrospun mesh embedded in a hydrogel matrix was developed as a ligament tissue engineering scaffold. These scaffolds were exposed to prolonged cyclic stretch to ensure that the scaffold was capable of withstanding elongation. The ECM production was analyzed to ensure deposition into the mesh and the presence of ligament ECM proteins. To study the impact of the hydrogel component on the composite meshes, cylindrical meshes were fabricated without the hydrogel component by rolling cell-seeded meshes into a cylinder and tying the ends, then

allowing the ECM produced by the cells to secure the layers of mesh. Again, the ECM production and mechanical properties were analyzed and compared to those of the hydrogel-electrospun mesh composite.

Ligament graft failure frequently results from poor integration of the graft with associated bone, so the final objective dealt with the development of the osteochondral interface critical to the appropriate transfer of load between ligament and bone in native ligament. It was hypothesized that a gradient of PDMS in an inorganic-organic scaffold would induce an osteochondral-like transition in cell phenotype.

CHAPTER II
BIOCOMPATIBILITY OF TINB SHAPE MEMORY ALLOY FOR BONE TISSUE ENGINEERING

2.1 Introduction

Between 2005 and 2030, demand for hip replacement surgeries is projected to rise by 174% to almost 600,000 procedures per year, and the estimated rise for knee replacements is 673% to 3.48 million yearly procedures.[44] These projections grossly underestimate the need for these surgeries, which is better reflected in hospital waiting lists. Joint replacement surgery is considered a highly successful procedure as measured by the reduction in pain and improvement in joint function, but as the number of procedures in younger patients rises, optimizing the success in terms of long-term survival of the prosthetic is required.[45] One approach to improving the long-term survival of a joint implant includes introducing pores into the material to promote bone ingrowth, which would stabilize the implant and reduce the loosening. Another approach involves developing materials that have similar mechanical properties to bone to reduce stress shielding and the subsequent bone loss.[28] Finally, ion release from metallic implants has been shown to cause loosening in joint replacements,[29] so the selection of a more biocompatible and corrosion resistant material may reduce the prevalence of this problem.

Metallic biomaterials such as titanium alloys, cobalt-chromium alloys, and stainless steels are used as implant materials for the replacement of structural components of the human body such as bones, joints, and tooth roots. Shape memory alloys (SMA) have the unique ability to recover their original shape upon heating and to sustain very large elastic strains, so they have been used for cardiovascular stents and medical and orthodontic wire.[46] The combination of shape memory effect and superelasticity can be applied for orthopedic tissue engineering as the superelasticity

allows the design of devices with constant stress over a wide range of strains[47], and this constant stress can accelerate healing.

With recoverable strains of up to 8%, titanium-nickel (NiTi) SMAs, also known as Nitinol, are the most popular SMAs used for biomedical applications. In applications involving contact of SMAs with live tissues, biocompatibility is crucial to the success of the implant material. The biocompatibility of NiTi alloys has been inferred from their high corrosion resistance[48-52] due to a stable and passive TiO_2 surface layer. This corrosion resistance depends on many factors though, and the malfunction of the 15 to 30% of stents which fail within 6 months of implantation[53-55] may be due, in part, to corrosion. Along with the TiO_2, there is also a small amount of elemental Ni in the surface layer of Nitinol.[56] The nickel content in these materials has been controversial, as elemental nickel has been shown to be toxic[57-59] and possibly carcinogenic.[60-62] Also, 4.5%[63] to 8%[64] of the general population are hypersensitive to nickel. Despite the nickel content, the results on the biocompatibility of Nitinol have been mixed. Multiple in vivo and in vitro studies have shown that Nitinol materials are at least as biocompatible as pure titanium.[56,57,65-70] Yet, several other studies have challenged the corrosion resistance and safety of NiTi alloys in the body.[53-55,71-77]

The concerns and unresolved issues associated with NiTi alloys, along with the growing need for implant materials, creates an urgent need for the design of nickel-free SMA with biocompatible constituents and better corrosion resistance. TiNb SMA systems have the potential to replace Nitinol in many applications. The most obvious advantage of TiNb SMAs over NiTi is the biocompatibility of all constituents.[78] The corrosion and wear resistance of TiNb has been shown to be superior to NiTi and Ti alone[78-81] since both Ti and Nb can form protective oxide layers. In addition, if this layer were to be compromised it was demonstrated that Nb will be spontaneously passivated due to its low anodic current potential.[81] Moreover, TiNb alloys are easy to process as compared to NiTi,[82] with good machinability, [83] and their sensitivity to compositional change is considerably less than that of NiTi.[84]

TiNb alloy systems can recover as much as 4.5% strain, [85] which although is less than the 8% recoverable strain that NiTi is capable of, should still be a suitable replacement for bone, which exhibits more than 1% recoverable strain. If deformation doesn't exceed the elastic limit, no damage to the material will result.[86] For standard metals such as stainless steel, elastic strain is so small that plastic strain is generated during normal wear. When plastic deformation accumulates, cracking and eventually failure will occur, but this should not be a problem if using TiNb for joint replacement applications. In its crystallographic orientation, TiNb alloys also possess very low Young's modulus, as low as 25 GPa,[80] which is very close to the 20GPa of bone,[87] and much lower than the 45-50 GPa modulus of NiTi single crystals.[80] This is advantageous for load bearing implants, such as in joint replacements, as stress shielding can cause bone atrophy and eventual failure of the implant.[28]

Porous materials are of importance for bone tissue engineering as they allow bone ingrowth and vascularization, which in turn provides a good integration/biological fixation of the biomaterial to the surrounding tissue.[88] Porous materials have benefits including low density, high surface area, and high permeability, which allows for cell attachment and then ingrowth of tissue into the metallic scaffold. A great deal of literature has covered porous NiTi SMAs, but with the increased surface area, porous materials pose an increased risk of cytotoxicity because of the increased potential for ion leaching. Therefore, the choice of non-toxic materials is of increased importance when designing porous materials. The study of porous TiNb alloys is still in its infancy, but these materials have the potential to become a promising scaffold for bone tissue engineering. A porous TiNbZr scaffold was fabricated with high levels of interconnected pores,[89] which is allows for cell growth and nutrient circulation.[90]

Before pursuing TiNb SMAs as a potential biomaterial or further processing it to develop porous TiNb or vascular stent materials, the biocompatibility and corrosion resistance must be verified at physiological conditions.

2.2 Materials and Methods

2.2.1 Metal and Alloy Preparation

$Ti_{74}Nb_{26}$ (Special Metals) and $Ni_{50.8}Ti_{49.2}$ (Sophisticated Alloys; at.%) alloys with 99.95% purity were produced using vacuum arc melting and were remelted four times to assure homogeneity. Commercial pure grade 2 titanium (OnlineMetals), and commercial pure niobium (Alfa Aesar), both with 99.5% purity were utilized as controls. Square pieces with dimensions of 10 mm x 10 mm x 1 mm were prepared, and then both sides of all specimens were mechanically polished to a final step in 0.05 micron colloidal silica and cleaned with ethanol.

2.2.2 Poly(ethylene glycol) Diacrylate Synthesis

Diacrylate-derivatized PEG (PEGDA) was prepared as previously described[91] by combining 0.1 mmol/mL dry PEG (3.4 kDa; Sigma), 0.4 mmol/mL acryloyl chloride, and 0.2 mmol/mL triethylamine in anhydrous dichloromethane (DCM; Fisher Scientific) and stirring at 4 °C under argon overnight. The resulting solution was washed with 2 M K_2CO_3 and separated into aqueous and DCM phases to remove HCl. The DCM phase was subsequently dried with anhydrous $MgSO_4$, and PEGDA was precipitated in diethyl ether, filtered, and dried under vacuum.

2.2.3 Cell Culture

Cryopreserved 3T3 cells (ATCC, Manassas, VA) at passages 4 were thawed and expanded at 37 ^{o}C and 5% CO_2. During expansion, cells were cultured in Dulbecco's Modified Eagle's medium (DMEM; Hyclone, Logan, UT) containing 10% iron-supplemented bovine calf serum (BCS; Hyclone), 100mU/mL penicillin, and 100mg/L streptomycin (Hyclone).

2.2.4 Short-term 2-D Culture Experiment

To understand the short-term cytotoxic effect of these metals, an experiment was designed to maintain cells in contact with alloy leachants yet separate from the alloy surface. In order to increase consistency of cell number between wells, mitomycin-c, an alkylating agent, was used to arrest the cell proliferation. This treatment ensured that confluence was not reached by the end of the study to increase the likelihood of full exposure of the cells to the ions produced from the alloy. The 3T3 cells, passage 8-9, were exposed to 8 μg/ml mitomycin C (Sigma) for 3 hours at 37 ^{o}C. The cells were then allowed to recover from this treatment overnight before being treated with 1 μM calcein AM (Invitrogen), which was used to monitor cell phenotype and viability during culture. The alloys and metal controls were sterilized by soaking for 3 hours in 70% ethanol, then the ethanol was removed and the samples were allowed to dry. Following the ethanol treatment, the metals were rinsed with PBS and then placed into the wells. The metals and cells were cultured with DMEM supplemented with 10% FBS, 100 mU/mL penicillin, and 100 mg/L streptomycin and maintained at 37 ^{o}C/5% CO_2. Culture media was collected for ion leaching analysis after 24, 48, and 72 hours of exposure. Cytotoxicity was assessed by LDH at the final time point.

2.2.5 Short-term2-D Experiment Analysis

Following 72 hours of culture, the cell culture inserts were treated with 1 mg/ml proteinase k in 1x TE buffer for 18 h at 37 ^{o}C to collect DNA. The DNA content was determined using the PicoGreen assay(Invitrogen).[92] DNA measures were translated to cell number using a conversion factor of 6.6 pg DNA per cell[93]. The cytotoxicity results were normalized by the cell number

2.2.6 Hydrogel Preparation

The behavior of cells is often dependent on culture conditions, as phenomena observed in two-dimensional culture are not necessarily observed in three dimensional culture. Therefore, to more closely mimic the environment in the body, a three-

dimensional study was designed with cells encapsulated in a PEGDA scaffold. The hydrogel precursor solution was prepared by dissolving PEGDA macromers in HEPES buffered saline (HBS; 10 mM HEPES, 150 mM NaCl, pH 7.4). Ten microliters of a 300 mg/mL solution of photoinitiator 2, 2-dimethoxy-2-phenyl-acetophenone dissolved in N-vinylpyrrolidone was then added per mL of precursor solution. ACRL-PEG-RGDS was added to the precursor solution so that the concentration of RGDS in the swollen hydrogels would be 1 μmol/g. The precursor solution then was sterilized using a 0.22 μm PVDF filter. 3T3 cells at passage 8–9 were harvested and resuspended in the hydrogel precursor solution such that the post-swelling cell density would be 2 X 10^6 cells/mL. Each solution was poured into molds composed of two glass plates separated by thin polycarbonate spacers and then polymerized by 2 min exposure to longwave UV light (Spectroline, ~6 mW/cm^2, 365 nm).

2.2.7 Long-term 3-D Culture Experiment

After 24 hours at 37 ^oC to allow the hydrogel to swell, an 8 mm biopsy punch (Miltex, York, PA) was used to cut uniform samples. Sterilized metal specimens (n=4 per formulation) were placed in 12 well plates, and the cell samples were placed in cell culture inserts.(BD Falcon, San Jose, CA). The gels and metals were immersed in DMEM supplemented with 10% FBS, 100 mU/mL penicillin, and 100 mg/L streptomycin and maintained at 37 ^oC/5% CO_2. Media was collected at the 24 hour time-point and then every 2 days for 14 days, and ICP-MS was performed at 24 hour, 7 day and 14 day time-points. The LDH cytotoxicity assay was performed following 14 days of culture.

2.2.8 Long-term 3-D Experiment Analyses

After 14-day total culture time, constructs were digested for 24 h at 37 °C in 1 ml of 0.1 M NaOH per 0.2 g hydrogel wet wt.[92] The samples were then centrifuged (10,000*g* for 10 min) and aliquots were taken for DNA quantification. The aliquots of the hydrolyzed samples (*n* = 4 per formulation) were neutralized and their DNA content

determined using the PicoGreen assay (Invitrogen)[92]. DNA measures were translated to cell number using a conversion factor of 6.6 pg DNA per cell[93]. Calf thymus DNA (Sigma) served as a standard.

2.2.9 LDH Cytotoxicity Assay

Lactase dehydrogenase(LDH), a metabolic enzyme present in the cytosol of the cell, can be used to quantify cytotoxicity, as the LDH is released from lysed cells. Consequently, an increased level of cell death would be accompanied by an increased concentration of LDH in the cell media. A colorimetric LDH assay, Cytotoxicity Detection Kit Plus (LDH) (Roche) was used to determine LDH activity in the cell media. Briefly, a 1:1 ratio of cell media to reaction mixture were applied to a 96 well plate and allowed to react for 20 minutes at room temperature. The stop mixture was then applied at a 1:5 ratio to the plate and the color development was detected using a microplate reader. After detection, the background controls were subtracted from the experimental values.

2.2.10 Microscopy

Alloys were imaged using optical microscopy prior to being exposed to cell culture media in static conditions. Following 72 hours exposure, the alloys were rinsed with ethanol and imaged again. These images were compared for any signs of corrosion.

2.2.11 ICP-MS

Media collected from the cell culture study were digested with sub-boiling HNO_3 (1:3 v/v) for 6 hours at 95 ^{o}C. This solution was then diluted 3:4 v/v with H_2O_2 and further digested for 2 hours at 95 ^{o}C. Digests were then diluted 1:10 in water. Four standards were prepared using digested media to obtain from 0 ppb to 100 ppb Ti, Ni, and Nb in the final dilution. Element specific detection was then performed on the standards and samples using a DRC II (Perk & Elmer/Sciex) Inductively Coupled Plasma Mass Spectrometry (ICP-MS). The regression coefficients obtained were

excellent(ranging from .9996 to 1.0000). A quality control was run between every four samples.

2.2.12 Potentiodynamic Measurements

Potentiodynamic tests were performed on TiNb, NiTi and Ti in both Hanks' physiological solution and 1M NaCl using a Pt counter electrode and an Ag/AgCl reference electrode. The potential scans were performed at a constant temperature of 37 ^{o}C. The scan rate was 4mV/s toward the anodic direction until 2000 mV.

2.3 Results and Discussion

The aim of the study was to assess and compare the cytotoxicity of TiNb alloys for biomedical applications to more commonly used NiTi alloy and analyze the corrosion resistance of the TiNb alloy. The cytotoxicity of the alloys and metals was determined using a lactate dehydrogenase (LDH) cytotoxicity assay. LDH is a metabolic enzyme present in the cytosol of the cell that can be used to quantify cytotoxicity, as the LDH is released from lysed cells. Therefore, an increased level of cell death would be accompanied by an increased concentration of LDH in the cell media. The corrosion resistance was assessed directly using potentiodynamic measurements of the metals and indirectly using ICP-MS of the cell media that was cultured with the alloys and controls. OM imaging of the metals was also used to visually inspect the materials before and after exposure to cell media for the short-term experiment.

A short term experiment was designed to put cells in direct contact with ions released from the metal into the cell culture media. This was a two-dimensional study where NIH 3T3 cells were cultured on well inserts while the alloys and control metals were in the same well. NIH 3T3 cells were selected because these cells are fairly resilient and often used for cytotoxicity assessments. Media was collected for cytotoxicity and ion leaching assessments every 24 hours for 3 consecutive days. The cells were treated with mitomycin C, which limits proliferation by blocking DNA and

RNA replication and protein synthesis. It is important to limit proliferation so that confluence is not reached by the end of the study to ensure full exposure to the ions produced from the alloy. **Figure 4- part A** shows the cytotoxicity results, normalized by cell number, for the short term cytotoxicity experiment. At the 72 hour time point, the cells cultured with the NiTi alloy showed elevated levels of LDH indicating increased cell death when compared to the biologically inert Ti. The cells cultured with the Nb control showed a similar level of cell death to the Ti control. These controls showed significantly lower levels of cell death than the NiTi alloy. The TiNb alloy caused slightly elevated cell death when compared to the Ti control in the short term study, but this wasn't statistically significant.

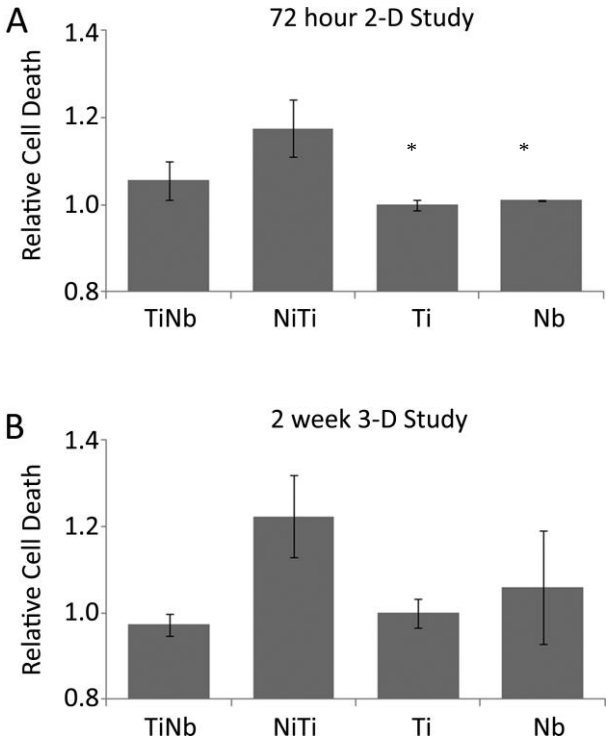

Figure 4: Cytotoxicity of TiNb alloy compared to NiTi, Ti, and Nb normalized by cell number. **(A)** 72 hour 2-dimensional study. *, significant difference from NiTi **(B)** 2 week 3-dimensional study

ICP-MS results for the short term experiment (**Table 1**) show an initial release of Ni from the NiTi alloy at 24 hours followed by a reduction in the Ni release at the 48 hour and 72 hour time points. This initial release caused prolonged death in the Ni samples as the 72 hour LDH measurement for the NiTi alloy was still greater than the TiNb alloy and the controls. The Nb control showed high levels of Nb at the 24 hour time point followed by a slight reduction in the Nb release levels, but there were still significant reading of Nb at 48 and 72 hours. These high levels of Nb didn't seem to affect cell behavior as the Nb control didn't have significantly more death than the Ti or TiNb samples. The TiNb sample didn't show significant leaching of Nb into the media at any time point.

Table 1: Ion release results for short-term experiment

	NiTi (PPB)			Nb (PPB)			TiNb (PPB)		
	24 hr	48 hr	72 hr	24 hr	48 hr	72 hr	24 hr	48 hr	72 hr
Nb	------	------	------	62.8 ± 2.7	24.2 ± 0.5	22.1 ± 1.7	4.0 ± 0.4	2.5 ± 0.3	1.2 ± 0.2
Ni	26.0 ± 3.8	3.9 ± 3.2	6.7 ± 5.1	------	------	------	------	------	------

Optical Microscopy (OM) imaging showed no signs of corrosion following the short term experiment even though an initial release of Ni occurred in the NiTi sample. Before and after OM images can be seen in **Figure 5**.

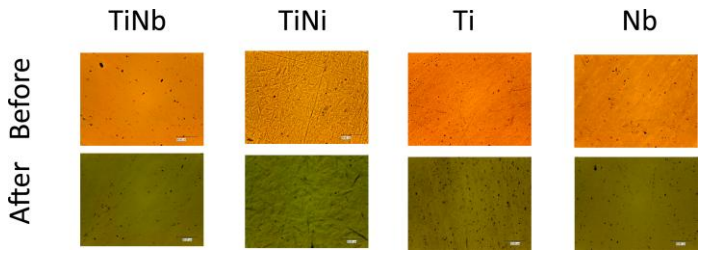

Figure 5: Optical microscopy images of metals and alloys before and after 72 hours culture. Scale bar=50 μm

The behavior of cells is often dependent on culture conditions, as phenomena observed in two-dimensional culture are not necessarily observed in three dimensional culture. Therefore, to more closely mimic the environment in the body, a three-dimensional study was designed with NIH 3T3 cells encapsulated in a PEGDA scaffold. Eight mm punches of PEGDA hydrogels were placed in well inserts and the metals were placed into the wells so media would be shared. Media was changed every 48 hours for two weeks. **Figure 4-part B** shows the cytotoxicity results for the long-term experiment, again normalized by cell number. At the 2 week time points, the cells cultured with the NiTi alloy and the Ni control again showed elevated levels of cell death when compared to the cells cultured with the Ti. Here, the Nb control showed a slight cytotoxic effect when compared to the Ti, but this effect was not statistically significant. The TiNb alloy caused a slight decrease in cytotoxicity when compared to the Ti control. Although the results were not statistically significant, the trends were similar in both the short and long-term study and the results were consistent at all of the time points analyzed.

Table 2: Ion release results for long-term experiment

	NiTi (PPB)		Nb (PPB)		TiNb (PPB)	
	1 wk	2 wk	1 wk	2 wk	1 wk	2 wk
Nb	------	------	1.3 ± 0.2	2.2 ± 0.7	0.2 ± 0.1	4.9 ± 0.6
Ni	2.1 ± 2.9	16.1 ± 9.04	------	------	------	------

Table 2 shows the ion leaching data for the long term study. At the one week and two week time points, the NiTi sample showed an insignificant level of Ni in the cell media after considering the noise in the two week time point. The amount of Nb leaching from the Nb and TiNb samples was also insignificant, indicating that under static conditions. In the NiTi samples, the ions seem to have an initial release at 24 hours (seen in the short-term study) followed by stabilization by 1 week. Although the levels of ions in the cell media wasn't considerable after the 24 hour time point for the NiTi alloy, the cytotoxicity results indicate that the effects of this initial Ni release are

prolonged because even at the two week time point, higher LDH levels indicate more cell death.

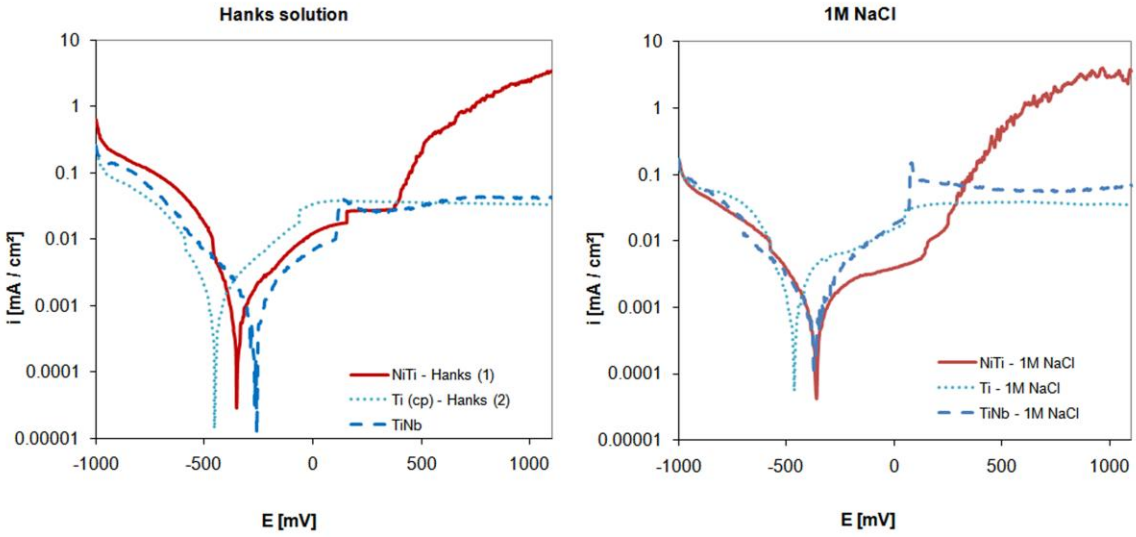

Figure 6: Potentiodynamic testing

Potentiodynamic testing was conducted to confirm the results seen in ICP-MS ion leaching. **Figure 6** shows the results of these corrosion tests in Hanks' buffered saline and 1 M NaCl. TiNb and Ti show similar passive corrosion behavior, while NiTi seems to reach a transpassive region upon anodic polarization. This indicates that Both Ti and TiNb exhibit superior corrosion resistance than NiTi.

The known toxicity of Ni has led to the controversy associated with the use of NiTi alloys for medical applications. Despite the presence of Ni, many researchers believe that NiTi alloys are biocompatible because of the corrosion resistance provided by a stable titanium oxide layer that limits the release of toxic Ni into the surroundings. Many studies that have shown NiTi to be biocompatible, yet others have raised concerns about cytotoxic effects and failure of NiTi devices. In both the short- and long-term experiments, the NiTi alloy was slightly more cytotoxic than the controls. Although the cytotoxicity results were not statistically significant, the trends were similar in both the short- and long-term study and the results were consistent at all of the time points

analyzed. Castleman et. al. observed in increase thickness of fibrous tissue after implantation in dogs. The thickness of this fibrous tissue is related to the degree of metal dissolution, so this indicates that metal was leaching into the surrounding tissue, challenging the biocompatibility of this material.[67] This is consistent with the ion leaching data for NiTi which shows that Ni is leaching out of the alloy before the oxide layer stabilized. This effect would just worsen with loading. The TiNb alloy showed similar levels of cell death as the control samples, which is consistent with the observations by Wang and Zhang.[94]

In addition to the lack of toxic constituents, TiNb has been shown to exhibit superior corrosion resistance to NiTi. Measures of corrosion through ion release and potentiodynamic testing showed just that. The NiTi samples showed an initial Ni release at the 24 hour time point before the oxide layer stabilized, while no significant level of Nb was measured from the TiNb alloy at any time point. Even with high levels of Nb leaching from the Nb control, no apparent cell death was observed, so if leaching of Nb from TiNb alloys occurred in dynamic conditions, it should not have a cytotoxic effect. It is also important to note that even with the low measured levels of Ni from the NiTi alloy, higher levels of LDH were measured during both experiments and this was repeatable. This is interesting as most literature pertaining to NiTi cytotoxicity depends on cell counting,[95] morphology,[96,97] and proliferation[98] as the main assessments of cell death, but this cytotoxicity assessment showed an elevation in LDH levels indicating a slight increase in cell death over the controls. Although the levels of ions in the cell media wasn't considerable after the 24 hour time point for the NiTi alloy, the cytotoxicity results indicate that the effects of this initial Ni release are prolonged because at endpoints of both experiments higher LDH levels indicate more cell death. Many researchers have worked on improving the oxide layer on NiTi alloys to improve the cytotoxicity behavior,[99] but these efforts would be compromised in dynamic conditions where these alloys will not only have to function in a corrosive environment but also under strain where the oxide layer can crack, causing higher levels on ion

release.[100] When the oxide layer cracks, the reconstruction of the passive film is a slow and difficult process.[101]

Following implantation into hard tissues, which is the case in joint replacements, the pH decreases to approximately 5.2 and recovers to 7.4 within 2 weeks.[102] Watari et al. showed that the amount of ions released from NiTi into Hanks' solution with pH 5 were larger than into saline indicating that the repassivation of the NiTi alloy is prevented by the inorganic ions present in the Hanks solution. The phosphate ions become incorporated in the surface oxide in the pH 5 Hanks' solution which delays the repassivation of the material, and eventually allows for an increase in the ion release.[103] This could cause the passivation time to extend for NiTi alloys after implantation and create a weaker oxide layer.

With improved corrosion resistance and the lack of toxic components, TiNb SMAs are promising replacements for NiTi. Future research should focus on the behavior of TiNb alloys in dynamic conditions and studying cell ingrowth in porous TiNb structures.

CHAPTER III
COMPOSITE HYDROGEL-ELECTROSPUN MESH SCAFFOLD FOR LIGAMENT TISSUE ENGINEERING*

3.1 Introduction

More than 150,000 ACL reconstruction surgeries are performed each year in the United States,[2] mostly in young, active individuals. Ligaments are dense fibrous tissue bands which connect two or more bones, guide joints through their normal range of motion, and maintain joint stability. Injury to these ligaments can range from minor disruption to the normal structure, to complete rupture of the tissue. This damage can result in pain and joint instability and eventually disease. The capacity for ligament tissue to recover from injury depends on many factors including location, mechanical forces they must withstand, and blood supply. Ligaments outside of joints, such as the medial collateral ligament will normally heal naturally[104] but ligaments that are within a joint, like the ACL, do not heal properly after damage because of limited vascularization and poor clotting ability.[104-106] Multiple treatment options exist for tears, but for ruptures, surgery is the primary option.[106] **Figure 7** shows the ACL during knee flexion, tension, and hyperextension.[107] In a study by Feagin, et al., both ends of ruptured ACLs were sutured together but after 5 years, were still not effectively fused and 94% of patients suffered from knee instability, demonstrating the limited healing potential of the ACL.[106] Therefore, the current treatment for rupture includes surgical removal of the ACL and replacement with a graft that is fixed to the bone on both ends.[108,109]

---

*Part of this chapter is reprinted with permission from "Hydrogel-Electrospun Mesh Composites for Coronary Artery Bypass Grafts" by McMahon RE, Qu X, Jimenez-Vergara AC, Bashur CA, Guelcher SA, Goldstein AS, Hahn MS, (in press) Tissue Engineering Part C. Copyright (2011) by Liebert Publishing Company

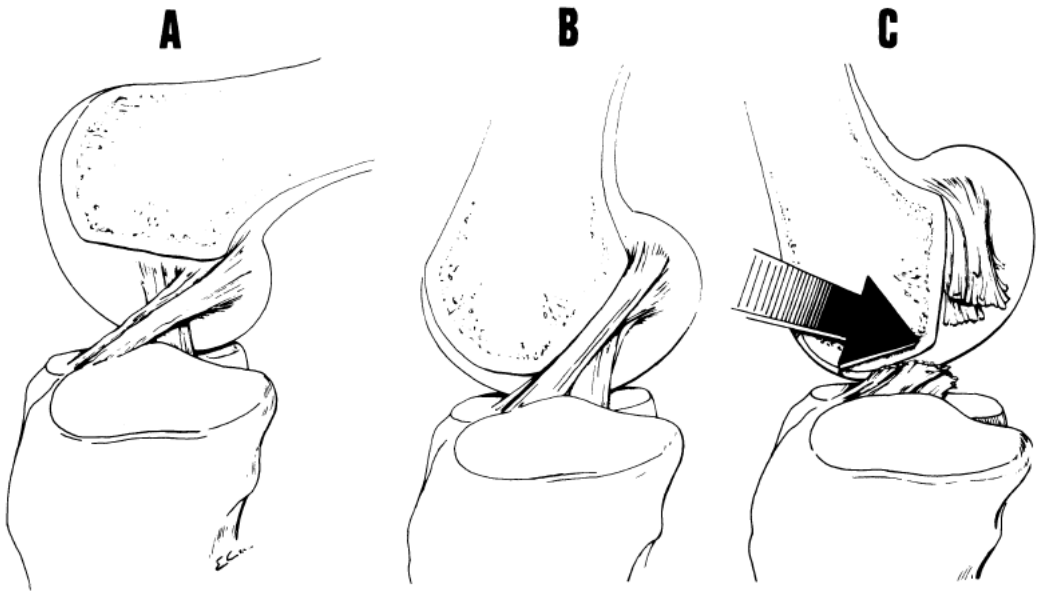

Figure 7: Bundles of the ACL. A) during knee flexion, B)during knee extension the ACL is taught, C) upon severe knee hyperextension, the ACL is torn by the femur [107]

The treatment for ligament damage generally includes surgery as more conservative treatments are often unsuccessful. The surgical treatment options include autografts, allografts, and synthetic grafts. Autografts are currently considered to be the best option. The quadriceps tendon or patellar tendon are often used for the autograft.[110,111] These risk the pain and donor site morbidity, which can cause muscle atrophy and tendonitis.[112,113] Allografts are limited by the availability of donor tissue, the risk of disease transmission,[114] and the potential for the tissue damage during storage. An immune response can occur in response to foreign proteins or cells in an allogenic graft which can trigger tissue rejection.[115] Dacron, Gore-Tex, and polypropylene based grafts which are non-biodegradable, have been developed but are currently not approved for ACL replacement because of low success rates, between 30 and 60%.[116]

Tissue engineering is a potential fourth option. A tissue engineering approach combines a biodegradable scaffold with autologous cells, such as mesenchymal stem cells that can differentiate into ligament fibroblasts and then induce tissue formation though the deposition of ECM.[117,118]

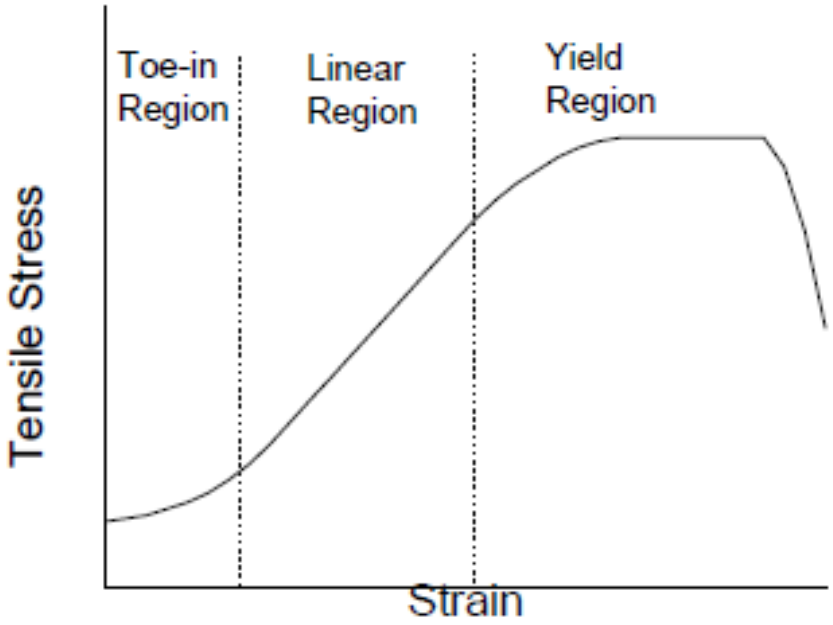

Figure 8: Ligament behavior under tensile load[119]

Native ligament exhibits three different regions of its stress-strain curve (the "toe-in" region, the linear region, and the yield region) during loading (**Figure 8**).[119] The crimped pattern of the collagen fibrils are straightened and elongated upon introduction of strain which creates the "toe-in" region.[113] After 2-4% strain the fibrils are elongated and stretching of the collagen triple helices and intrafibrillar slippage between crosslinks occurs causing the linear region.[119-121] The failure of ligament tissue generally occurs between 7 to 16% strain. During normal movement, the ACL is typically stretched 4-5%, through the "toe-in" region and part of the linear region[122] and the typical ACL is able to withstand the loads associated with normal activity because it has a modulus of about 111 MPa.

Electospun meshes have been identified as a potential scaffold for tissue engineering of ligaments as they can possess the high tensile properties necessary for replacing ligament. Electrospinning is a common method for fabricating fibrous non-woven meshes with high tensile strength and open porous structures.[123] Electrospun

fibers can be oriented by electrospinning onto a rotating drum[124] and the fiber diameters produced in the range of 100 nm to 7 um.[125-128] Oriented meshes have the ability to align cells through a phenomenon called contact guidance and these oriented cells will deposit oriented ECM.[129-131] This is important because oriented ECM has higher tensile strength than unoriented ECM like scar tissue.[132] Mesh thickness is controlled primarily by the length of time for electrospinning and typically ranges from 140 um to .5 mm.[133-135] Thicker scaffolds can be produced, but this isn't practical because producing a thickness of 1 mm requires many hours of electrospinning.[136] Therefore, a scaffold that maintains high tensile strength of electrospun scaffolds while bringing the thickness of the constructs nearer to that of native ligament would be desired.

One possible approach to achieving these dual design goals is to form a composite consisting of electrospun fiber mesh layers bonded together by a hydrogel matrix. Hydrogels generally have initial tensile moduli and strengths significantly below those of native ligament.[137] Therefore, the composite scaffold would be expected to have mechanical properties intermediate between that of the electrospun layers and the hydrogel adhesive. In the present work, we validated this approach by using a poly(ester urethane) urea (PEUUR)-based electrospun mesh and a poly(ethylene glycol) (PEG)-modified fibrin hydrogel. PEUURs are a family of biodegradable, biocompatible, elastomers[138,139] with mechanical properties (i.e., elastic modulus, strain to failure, ultimate tensile strength, and degradation rate) that can be varied over a broad range by careful control of the chemistry and molecular weight (M_w) of the individual PEUUR segments.[138,140,141] Concurrently, fibrin gels are known to be adhesive[142] and appear to support the elastogenesis important to the maintenance of long-term graft mechanical properties.[143] Further, the grafting of PEG chains to these hydrogel networks slows their degradation,[144] reduces their thrombogenicity,[145] and can enhance their initial mechanical properties. In the current study, we demonstrate that fibrin gel-PEUUR mesh composites can be fabricated with circumferential moduli and tensile strengths in the range of native vasculature. In addition, we show that the resulting constructs support

extracellular matrix (ECM) accumulation and maintain their mechanical integrity following prolonged cyclic stretching.

3.2 Materials and Methods

3.2.1 Polyurethane Synthesis

A linear segmented degradable PEUUR elastomer, consisting of alternating a PCL soft segment and a urethane- and urea-containing hard segment, was synthesized using a standard two-step technique in a three-neck, round-bottom flask equipped with argon inlet and outlet, condenser, and stirrer.[146] First, the flask was charged with anhydrous dimethyl sulfoxide (DMSO, <50 ppm water; Acros Organics) and 1,6-diisocyanatohexane (HDI; Sigma-Aldrich), immersed in a 75 ^{o}C oil bath, purged with argon, and constantly stirred. Next, PCL diol (average molecular weight 2000 Da, PCL2000; Sigma,) that had been dried for 24 h at 80 °C under vacuum (10 mmHg) and dissolved in DMSO was charged into the reactor by means of an addition funnel. The prepolymer content in the reactor was controlled at 14 wt%, and the relative masses of HDI and PCL2000 were selected to achieve a prepolymer NCO:OH equivalent ratio of 2.0:1.0. Dibutyltin dilaurate (Sigma) was added to the flask at 1000 ppm, and the reaction was allowed to proceed for 3 h to produce a HDI.PCL2000.HDI prepolymer. In the second step, a solution of 1,3-propanediol bis(4-aminobenzoate) (Sigma-Aldrich) in DMSO was prepared at 50 °C and added to the resultant prepolymer in the reaction vessel. The NCO:OH equivalent ratio of the polyurethane was controlled at 1.03:1.0, and the polymer concentration was 12 wt%. Dibutyltin dilaurate was added to a concentration of 1000 ppm. The reaction was allowed to proceed at 80^{o}C for 20 h. The final polymer was then precipitated in diethyl ether (Sigma) and dried for 24 h at 8 °C under vacuum.

3.2.2 Electrospinning Procedure

The PEUUR was electrospun to form fused-fiber meshes with controlled fiber

diameter and fiber alignment as described previously.[147],[148] Briefly, electrospinning was performed with a 10 wt% PEUUR2000 solution in 50:50 isopropanol:1,1,1,3,3,3-hexaflouro-2-propanol (HFIP; Sigma) using a 22-gauge Teflon tipped needle, a 15 kV potential, a throw distance of 15 cm, and a syringe flow rate of 5 mL/h. A 6-cm-diameter drum rotating at a linear velocity of 8 m/s served as the collector. Meshes (150-200 μm thickness) were removed from the drum and soaked in ethanol for 7 days followed by deionized water for 2 days to remove residual HFIP. The meshes were then dried and stored in a desiccator until use. The meshes were sterilized by γ-irradiation at the Wake Forest Institute for Regenerative Medicine.

3.2.3 Mechanical Testing of Electrospun Mesh

The tensile moduli of electrospun PEUUR meshes were determined using 15×10 mm strips that had been soaked in PBS overnight before testing. The thickness of the meshes was on the order of 0.1-0.2 mm and therefore could not be accurately measured with calipers. Instead thickness was estimated from measurements of mesh mass, length, width and density (1.13 g/cm^3) using an assumed porosity of 60%[133]. The segments were exposed to uniaxial strain at a rate of 6 mm/min until failure. Modulus was calculated from the linear region of the stress strain curve (typically between 25 and 45% strain) using a cross-sectional area based on an assumed 60% mesh porosity. Results are presented as mean ± standard deviation for n=3 meshes.

3.2.4 Scanning Electron Microscopy

The mean fiber diameter and angular deviation were determined to by quantitative analysis of SEM images per Bashur et al.[149] Briefly, electrospun meshes were mounted onto studs and sputtercoated with a 10nm layer of palladium (Model 208HR, Cressington Scientific Instruments,). Images were acquired using a LEO 1550 Field Emission SEM (Carl Zeiss SMT) operating at 5kV with a 16mm working distance. Resultant images were imported into ImagePro Plus software (ICube,) for analysis of fiber diameter and fiber orientation. Fiber diameter and angle of orientation (relative to

the vertical axis of the image) was determined manually. The degree of orientation was characterized by the angular standard deviation, σ, for a wrapped normal distribution:

$$f(\theta) = \frac{1}{\pi}\left(1 + 2\sum_{p=1}^{\infty} \rho^{p^2} \cos(2p(\theta - \mu))\right).$$

Here, the probability distribution function has been adapted from Fisher[150] for a periodicity of π radians, where μ is the mean angle and ρ is the mean resultant length. These parameters were determined from a set of n measured fiber orientations, θ_i, by the following equations:

$$\rho = \frac{1}{n}\sqrt{\left(\sum_{i=1}^{n} \cos 2\theta_i\right)^2 + \left(\sum_{i=1}^{n} \sin 2\theta_i\right)^2},$$

$$\mu = \tan^{-1}\left(\sum_{i=1}^{n} \sin 2\theta_i \Big/ \sum_{i=1}^{n} \cos 2\theta_i\right).$$

Finally, the angular standard deviation was calculated from the mean resultant length:

$$\sigma = \frac{1}{2}\sqrt{-2\ln \rho}.$$

3.2.5 Poly(ethylene glycol) Diacrylate Synthesis

Diacrylate-derivatized PEG (PEGDA) was prepared as previously described[91] by combining 0.1 mmol/mL dry PEG (3.4 kDa; Sigma), 0.4 mmol/mL acryloyl chloride, and 0.2 mmol/mL triethylamine in anhydrous dichloromethane (DCM; Fisher Scientific) and stirring at 4 °C under argon overnight. The resulting solution was washed with 2 M K_2CO_3 and separated into aqueous and DCM phases to remove HCl. The DCM phase was subsequently dried with anhydrous $MgSO_4$, and PEGDA was precipitated in diethyl ether, filtered, and dried under vacuum.

3.2.6 Cell Culture

Mouse smooth muscle progenitor cells (10T½, American Type Culture Collection) at passage 2 were thawed and expanded at 37 °C and 5% CO_2. During expansion, cells were cultured in Dulbecco's Modified Eagle's medium (DMEM; Hyclone) containing 10% heat-inactivated fetal bovine serum (FBS; Hyclone). Cells were harvested for seeding and/or encapsulation between passages 10 and 12.

3.2.7 Construct Fabrication

To fabricate cylindrical constructs, molds consisting of a Teflon base, an inner hollow latex tube (0.125" OD, 0.015" wall thickness; Kent Elastomers) supported by a 2 mm glass rod, and an outer hollow cylinder of Teflon (0.25" ID, 0.012" wall thickness; Small Parts, Inc.) were used. All mold components were sterilized by autoclaving. Latex tubing was used as an inner mandrel of the mold per Syedain et al.[151] to aid in the formation of a tight-seal when mounting of the constructs on bioreactor ports. Each construct was fabricated in a two-step process, the first involving fibrin gel-mesh preparation and the second involving PEG grafting to the fibrin component of the resulting constructs.

3.2.8 Fabrication of PEG Grafted Fibrin-Mesh Composites

Rectangular segments (2 cm × 3.5 cm) were cut parallel to the direction of fiber orientation from the 150-200 μm thick mesh. Next, each mesh segment was exposed to media containing 40% serum overnight at room temperature to improve cell adhesion. The coated mesh segments were then rinsed with PBS, and cells were seeded on the upper mesh surface at 10^4 cells/cm^2. Following two days of culture, the cell-laden meshes were rolled around the latex mandrels (**Figure 9- part A**), resulting in 2 to 3 layers of mesh and a mean circumferential orientation of the mesh fibers. During the rolling processes, the cell layer faced outward and mesh segments were handled only at the edges to limit mechanical removal of seeded cells. A sterile 3.1 wt% fibrinogen solution containing 5 U/ml thrombin and $5x10^6$ 10T½ cells per mL was then prepared and pipetted around the inner mesh-wrapped mandrel. This fibrinogen solution impregnated the layers of rolled mesh as it polymerized, resulting in a cohesive fibrin gel-electrospun mesh composite. Following 30 minutes incubation at room temperature, the constructs were removed from the molds and immersed in PBS containing 1.3 U/mL thrombin, 0.5 wt% 3.4 kDa PEGDA, and 0.26% Irgacure 2959. After 1 hour at 37 °C, the constructs were removed from the solution, and exposed to longwave UV light (~10 mW/cm^2, UVP) for 5 minutes. The purpose of this extended thrombin exposure followed

by vinyl-mediated PEG grafting was to slow the rate of fibrin degradation through increased fibrin crosslinking (achieved through additional exposure to thrombin). In addition, conjugation of PEG chains to proteins has been demonstrated to reduce the rate of protein degradation[144] and to decrease thrombogenicity.[145] PEGDA was not added to the initial fibrinogen solution, since it tended to induce irregular clotting of the fibrinogen on addition of thrombin. The PEG-grafted fibrin-mesh composite (PEG-FB-mesh) constructs (~15 mm length, ~5.5 mm O.D., ~1mm thickness) were then immersed in media containing 10% FBS and 1% PSA (10,000 U/mL penicillin, 10 g/L streptomycin, and 25 mg/L amphotericin, Mediatech).

3.2.9 Cell Viability Analysis

To confirm the cytocompatibility of the extended thrombin-PEGDA exposure associated with hybrid gel-mesh construct fabrication, LIVE-DEAD staining (Invitrogen) was performed per standard protocols for n = 3 specimens.

3.2.10 SEM Analysis of Composites

To examine the interpenetration of the fibrin gel and electrospun mesh components of the composite constructs, ring segments were fixed in 10% acrolein (Sigma) and dehydrated with a graded ethanol series (5-100%) with intermittent vacuum in a PELCO Biowave® microwave system (Ted Pella, Inc.) at 200 W and 10 °C. One min microwave cycles were used for dehydration until 50% ethanol, after which 6 min cycles were used to complete the dehydration process. Final dehydration consisted of three changes of 100% ethanol with intermittent vacuum and 6 min microwave cycles. Ethanol was then replaced with three changes of hexamethyldisilizane (Electron Microscopy Sciences) followed by the intermittent vacuum and microwave cycles. The resulting ring segments were mounted along their base onto stubs, after which they were exposed to ruthenium tetroxide vapor (Sigma), sputtercoated with Au:Pd (60:40), and imaged in a JEOL 6400 SEM equipped with a tungsten filament at an accelerating voltage of 10 kV.

3.2.11 Construct Integrity Following Mechanical Conditioning

After two days static culture, 1 ng/ml transforming growth factor β1 (TGF-β1; Sigma) was added to the culture media to promote 10T½ differentiation into smooth muscle like-cells.[147] Following a total of 4 days of static culture, each construct was cut in half using surgical scissors. One half of each construct was randomly assigned for dynamic culture (n = 4), while the remaining portion was allocated for static culture (n = 4). Dynamic constructs were mounted in a modification of the pulsatile flow bioreactor previously described in Bulick et al.[137] Because bioreactors are expensive to design and must be validated, the constructs were mounted on a bioreactor designed for vascular grafts. The electrospun mesh fibers were oriented in the direction of the strain (circumferentially) and experienced a 2% strain for 12 days.

During the period of mechanical conditioning, both static and dynamic constructs were cultured in DMEM, 10% FBS, 1% PSA, 1 ng/mL TGF-β1, with 2 mg/mL ε-aminocaproic acid to slow the degradation of the fibrin, and 50 μg/ml ascorbic acid added to increase collagen production. Media was changed for all constructs every two days for 12 days.

3.2.12 Construct Analyses

After 16 days total culture time, the static and dynamic constructs were harvested for biochemical and histological analyses. Each PEG-fibrin-mesh construct was cut into 5 ring segments, each ~3-5 mm in length, and the latex tubing was gently removed. The two end-segments were discarded. One segment per construct was allocated for mechanical testing. The remaining sections were immersed in formalin overnight, after which they were allocated for histological or biochemical assays. Details of the mechanical testing, and biochemical and histological analyses are given in the following sections.

3.2.13 Mechanical Property Assessment

The mechanical properties of the hydrogel-mesh composites were measured at time zero and following 16 days of culture. For mechanical property assessments, 3-5 mm ring segments were cut using surgical scissors from constructs that had been immersed in media overnight. Circumferential mechanical tests were performed using a modification of the technique validated in Johnson et al.[91] Calipers were used to measure the dimensions of each construct segment. Each ring was then mounted onto an Instron 3342 equipped with a 10 N load cell using custom brackets.[137] The ring segments were exposed to uniaxial strain at a rate of 6 mm/min until failure. Applied stress was calculated from the measured force by approximating the area of force application as two rectangles, each with sides equal to the width and wall thickness of the ring. The gauge length, l_g, was taken as the inner diameter, D_v, of the unstretched ring plus the wall thickness, h_v. The incremental or tangential modulus, E, of each sample was defined as the slope of the resulting stress–strain curve at a reference stress of 20 kPa to mimic the circumferential stress experienced by vessels under physiological pressures (~0.5 P_{avg} D_v /h_v).[152] The ultimate tensile strength (UTS) of the samples was defined as the maximum stress applied prior to failure.

3.2.14 Biochemical Analyses

Samples for biochemical analyses were transferred to 2 mL screw-cap microfuge tubes containing 1.5 ml of lysis buffer (PBS containing 1% Triton X-100 (Fisher), 0.5% sodium dodecyl sulfate (Sigma), and 100 µg/mL phenylmethanesulfonylfluoride (Sigma)) and 1 mL of 3.2 mm stainless steel beads. Each sample segment was homogenized at 4800 rpm in a Bead-Beater homogenizer (Biospec) in 10 s cycles with 1 min intermediate cooling on ice. Each sample was analyzed via competitive ELISA for (ECM) proteins collagen I (COL1A1; clone D-13) and collagen III (COL3A1; clone S-17) and housekeeping protein GAPDH (clone V-18). In brief, peptides corresponding to the immunogen for each antibody were obtained from Santa Cruz Biotechnology (SCBT) and used to coat EIA plates (Costar) at either 500 ng (collagen III peptides) or

2000 ng (collagen I and GAPDH peptides) per well, after which the wells were blocked with bovine serum albumin (BSA). At the time of analysis, samples were incubated with primary antibody (SCBT) for 1 h, after which the sample-antibody mixtures were applied to the coated plates for 1 h. Standards were prepared by similarly incubating primary antibody with varying levels of immunogen peptide for 1 h, followed by application to coated plates. For both samples and standards, bound primary antibody was detected using an appropriate HRP-conjugated secondary antibody (Jackson Immunoresearch), followed by application of 2,2'-azino-bis(3-ethylbenzthiazoline-6-sulphonic acid) (Sigma) and monitoring of absorbance at 410 nm.

3.2.15 Histological Analyses

Histological sections were fixed in formalin overnight at 4 °C, embedded in OCT media, and cut into 10 μm sections using a CryoJane Tape Transfer system (Instrumedics). This system allowed the sections to be anchored to the slide to retain construct structural integrity during the immunostaining process. ECM deposition and cell phenotype were analyzed in 2 sections per sample using standard immunohistochemical techniques. In brief, rehydrated sections were blocked by 30 min exposure to Terminator (Biocare Medical). Primary antibodies for elastin (BA-4; Sigma), collagen I (Rockland Immunochemicals), collagen III (Rockland Immunochemicals) were diluted in PBS containing 3 % BSA and 0.5 % Tween 20 and applied overnight at 4 °C. Bound primary antibody was detected either by using the appropriate HRP-conjugated secondary antibody (Jackson Immunoresearch) followed by application of the chromogen 3,3’-Diaminobenzidine (DAB; SCBT). Sections were then dehydrated with graded alcohol followed by xylene, and then mounted using Polymount (Polysciences) or Curemount (Instrumedics). Stained sections were imaged using an Axiovert microscope (Zeiss).

3.2.16 Statistical Analyses

Data are reported as mean ± standard error of the mean. Comparison of sample means was performed by one-way ANOVA, $p < 0.05$.

3.3 Results and Discussion

Composite hydrogel-electrospun mesh scaffolds were generated by rolling a PEUUR electrospun mesh around an inner mandrel and then binding the juxtaposed layers together using a fibrin-based hydrogel. Mouse mesenchymal progenitor cells, 10T1/2, which have the ability to differentiate into ligament fibroblasts, were seeded onto the electrospun mesh 4 days before rolling and suspended in the fibrin hydrogel to ensure even distribution throughout the construct. This process resulted in a cylindrical construct with multiple layers of electrospun mesh and hydrogel between and throughout, as seen in **Figure 9**. After 16 days total culture time, mechanical testing was performed and biochemical and histological analyses were completed to determine the feasibility of this composite system as a tissue engineered ligament graft.

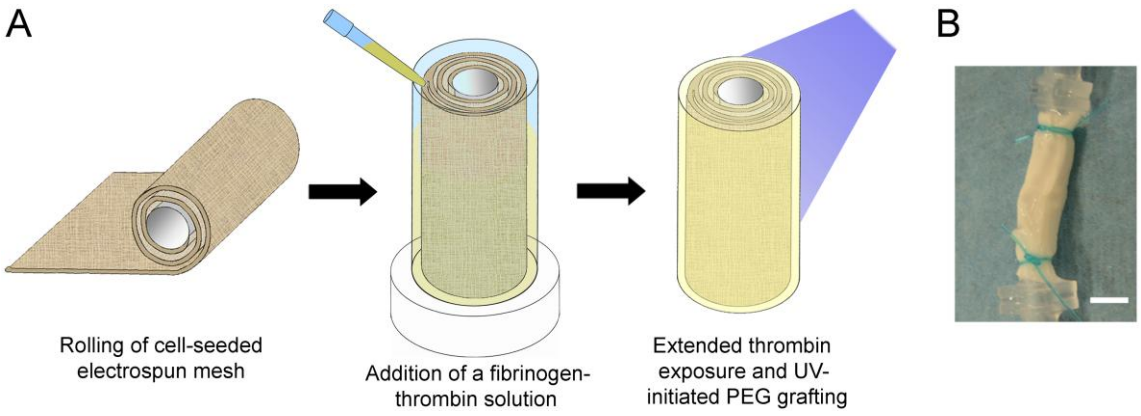

Figure 9: Construct fabrication. **(A)**A wetted electrospun mesh wrapped around the latex mandrel of a construct mold. An outer thin walled PTFE hollow cylinder was then placed around the wrapped mandrel. After fibrinogen-thrombin solution was pipetted into the mold and allowed to set, a hydrogel-mesh hybrid construct resulted. **(B)** Resultant layered hydrogel-electrospun mesh structure. Scale bar = 5 mm.

Fluorescence imaging was used to confirm the ability of acrylate (ACRL)-terminated PEG to graft to fibrin hydrogel networks. A monoacrylate-derivatized PEG molecule (ACRL-PEG-lysine) was prepared for these assays. Conjugation of the PEG to lysine permitted the introduction of a fluorescent label using standard NHS chemistry. The intensity of the fluorescence in **Figure 10- part C** is much higher than the controls (**Figure 10-parts A and B**), indicating that the (ACRL)-terminated PEG did in fact have the ability to graft to the fibrin networks.

Figure 10: Confirmation of the ability of acrylate (ACRL)-terminated PEG to graft to fibrin hydrogel networks. All images were obtained using the FITC fluorescence channel of a Zeiss Axiovert microscope. (A) A representative image of a pure fibrin gel. (B) A representative image of a fibrin gel exposed to photoinitiator and longwave UV light but not to AlexaFluor 488-labeled ACRL-PEG-lysine. (C) A representative image of a fibrin gel exposed to photoinitiator and 0.5 wt% AlexaFluor 488-labeled ACRL-PEG-lysine followed by longwave UV light. The hydrogels in (B) and (C) were immersed in PBS overnight followed by several rinses in PBS prior to imaging to ensure removal of unconjugated species. The scale bar in (A) applies to all images and represents 50 μm.

In addition to providing the "toe-in" region associated with the composite scaffold, the PEG-fibrin hydrogel was intended to act as an adhesive agent, effectively bonding successive mesh layers together. To serve as an effective bonding agent, the fibrin hydrogel should penetrate into the electrospun mesh layers. SEM imaging was therefore conducted to assess the microstructure of the PEG-FB-mesh composites. The resulting images indicate that the chosen construct fabrication conditions supported the hydrogel-mesh interpenetration required for construct integrity and for the effective transfer of load between scaffold components (**Figure 11- parts B-C**). To confirm the cytocompatibility of the extended exposure to thrombin, PEGDA, and photoinitiator associated with construct generation, the LIVE-DEAD assay was performed on scaffold segments (**Figure 11– part D**). These studies indicated a 24 h post-fabrication cell

viability of 75 ± 2%, a level consistent with that observed following cell encapsulation within PEGDA gels.[153]

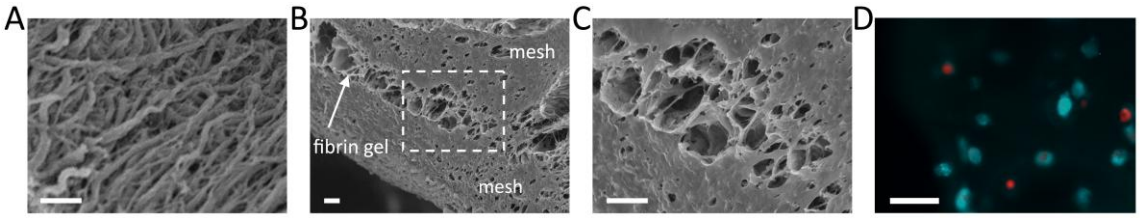

Figure 11: Construct structural integrity and cell viability. (A) An SEM image of a single electrospun mesh layer illustrating fiber thickness and orientation. (B) An SEM image of a transverse cross-section through a hydrogel-electrospun mesh construct indicating effective bonding and interpenetration between the hydrogel and mesh layers. In preparation for SEM imaging, the inter-layer bond withstood dehydration (which differentially impacts hydrogel and mesh components) as well as multiple microwave cycles. (C) A higher magnification image of the boxed region of the hydrogel-mesh construct shown in (B). (D) A representative fluorescence image of LIVE (green)-DEAD (red) stained cells within the fibrin gel portion of the hybrid constructs at 24 h post-fabrication. As shown in (D), cells encapsulated within the fibrin hydrogel had not yet fully spread following 24 h of culture. The scale bars in (A)-(C) represent 10 μm and the scale bar in (D) represents 40 μm.

To determine the shape of the stress-strain curve of the composite scaffold, tensile testing in the direction of the fibers was performed at time zero and following 16 days total culture. **Figure 12- part A** shows a typical stress-strain curve for tensile testing on PEG-FB-mesh composite scaffold following 14 days of static culture. There is a "toe in" region, followed by a linear region, and then the onset of failure, similar to the ligament. **Figure 12- part B** compares this behavior to that of pure electrospun ring sample. The pure electrospun mesh scaffold did not exhibit a "toe-in" region as seen in typical ligament tissue. Therefore, the composite scaffold seems to exhibit behavior of both components of the scaffold creating a scaffold with properties which better mimic native ligament.

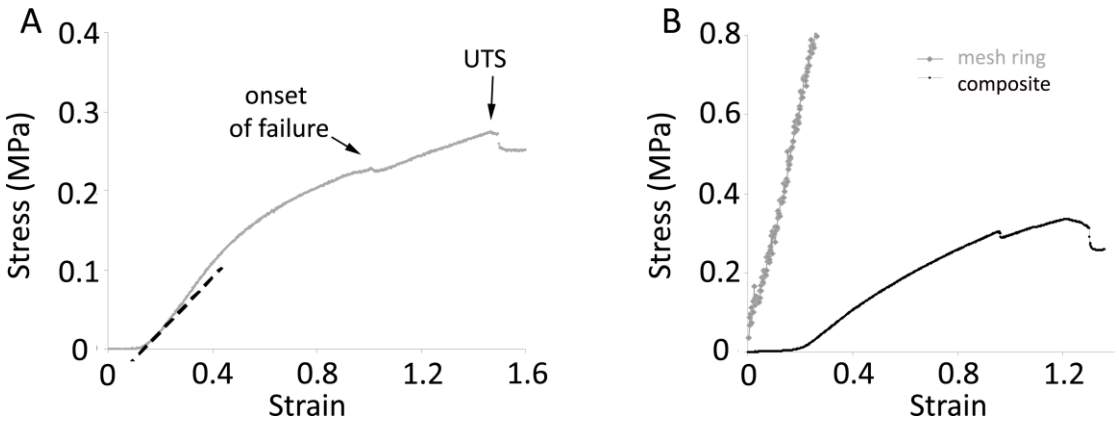

Figure 12: Mechanical testing. (A) A representative ring test of a PEG-fibrin-mesh construct following 14 days of static culture (B) A representative time 0 PEG-fibrin-mesh composite scaffold compared to a time 0 pure mesh ring

In order to examine cell phenotype and ECM production, competitive ELISA assays and immunohistology were performed on PEG-FB-mesh composites. Since the ECM of the ligament is mainly composed of collagen I and collagen III, as well as elastin, these ECM markers were examined. Contrary to expectations, COL1A1 and COL3A1 appeared unchanged by mechanical conditioning when analyzed using competitive ELISA (**Figure 13- part A**). Both collagen I and collagen III would be expected to be elevated in mechanical conditioned constructs.[92,148,151,154] However, elastin deposition appeared to increase with mechanical conditioning, although this trend fell below statistical significance. Increased elastin production[92,148,151,154] is generally associated with cyclic distension. Histology supported the trends for ECM production (**Fig 13- part B**) and these proteins were able to diffuse through and deposit into the mesh.

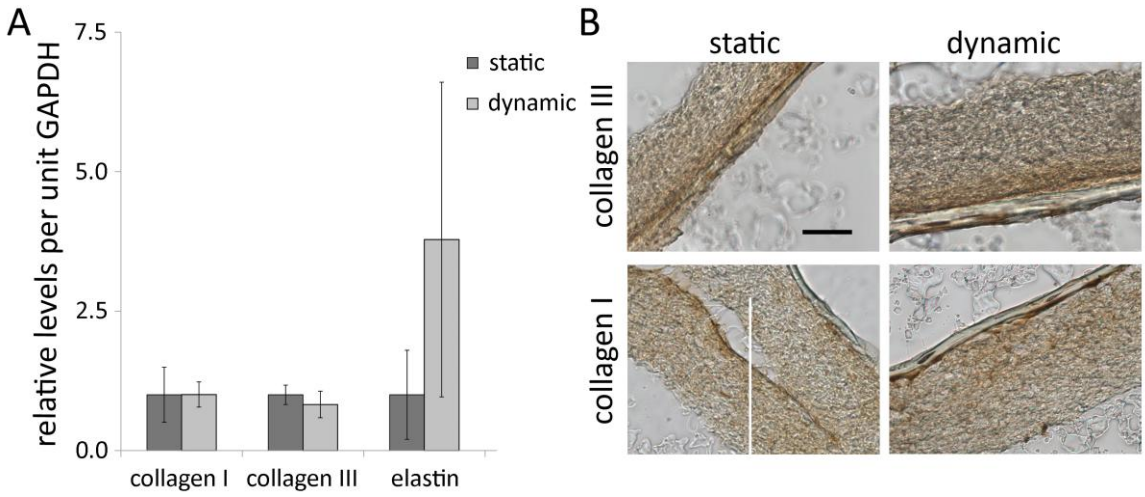

Figure 13: Immunostaining and biochemical comparison of static and mechanically conditioned PEG-fibrin-mesh constructs. (A) ELISA results for COL1A1, COL3A1, elastin per unit GAPDH. (B) Representative images of collagen type III and collagen type I immunostained sections. The scale bar applies to all images and represents 50 µm.

For hydrogel-mesh composites to maintain appropriate mechanical properties over the long-term, however, the loss of construct stiffness and strength due to mesh and/or fibrin degradation or to the hydrogel-mesh bond must be offset by neomatrix production. Ideally, the cells and deposited matrix will be distributed throughout the scaffold. Immunostaining for collagen I and collagen III (**Figure 13- part B**) showed protein deposition in the meshes with a higher concentration near the edges of the gel as indicated by darker staining. This is a good indication that more cells are located toward the edges of the meshes but they can deposit proteins further into the scaffold.

The tensile modulus of the oriented PEUUR electrospun mesh used herein parallel to the fiber orientation was approximately 690 kPa, which is much lower than the 111 MPa modulus of native ligament. The initial circumferential modulus was determined to be 314 ± 17 kPa, and was unchanged following 16 days total of either static or dynamic culture. Although these properties would not be suitable for use in ligament tissue engineering, this method produced a graft which could withstand prolonged cyclic stretching and had dimensions suitable for implantation. Since both the mechanical properties of the electrospun mesh and fibrin gel can be broadly tuned, we

anticipate that the tuning of the scaffold formulation will result in a composite graft which better matches desired graft properties. For example, Huang et al. developed a method to electrospin a synthetic sequence of elastin that resulted in a dried nanofiber mesh with a Young's modulus of 1.8 GPa.[155] The current research shows that the mechanical properties of the electrospun mesh can be modulated by fabricating a composite scaffold with a hydrogel, so selection of the electrospun component with a higher tensile strength could produce a scaffold with mechanical properties suitable for implantation, yet retaining the other benefits from the design on the composite scaffold.

Mechanical testing of PEG-FB-mesh scaffolds suggests that the mechanical integrity of these constructs is robust under both prolonged static culture and physiological pulsation. However, the variance in the observed moduli and UTS among samples within a given treatment group increased notably with culture in both static and dynamic culture. In addition, cyclic pulsation appeared to be resulting in a more rapid reduction in the UTS relative to static culture, although this trend was not statistically significant. The properties of the composite scaffolds seem to be highly correlated with the integrity of the fibrin glue bond between each adjacent mesh layer. The integrity of this fibrin bond can be reduced by fibrin or mesh degradation and/or mechanical shearing. Thus, if dynamic conditioning is indeed resulting in a reduction in UTS, the mechanical shear between bonded fibrin-mesh layers induced by repeated distension may underlie this reduction.

This project showed the feasibility of composite electrospun mesh-hydrogel composites for tissue engineered ligament grafts. These composite systems warrant further study as they can be applied for regeneration of not only ligament, but many other oriented tissues such as vascular or neural.

CHAPTER IV
COMPOSITE EXTRACELLULAR MATRIX-ELECTROSPUN MESH SCAFFOLD FOR LIGAMENT TISSUE ENGINEERING

4.1 Introduction

Recently, in order to try to use the ECM produced by cells as the main scaffold for tissue engineering and to bypass the drawbacks associated with traditional scaffolds, researchers have been trying to apply cell sheets for ligament[156] tissue engineering. Most tissue engineering approaches involve culturing cells on tissue culture plastic until the necessary number is obtained, followed by enzymatic digestion (trypsin) to prepare a suspension of single cells. These cells are encapsulated or seeded onto a scaffold. The disadvantage to this method includes the loss of many cells during the process of seeding onto scaffolds as many cells do not adhere to the scaffold, but seep through the pores.[157-159] The cells that do adhere must then produce new ECM, and the loss of cellular activity due to changes in chemical makeup and morphology of cells may be attributed to trypsinization.[160]

Researchers have successfully layered multiple two-dimensional sheets of adult cells to create a three dimensional tissue.[161-163] but these cells have limited lifespan, differentiation potential, and require long culture times to produce a cell sheet with ECM strong enough to be handled. Mesenchymal stem cells have the capability of differentiating toward ligament cells,[120] and have better collagen secretion and proliferative capacity than mature collateral ligament, ACL, and skin fibroblasts.[164,165] Sheets of bone-marrow derived MSC were grown and shown to be viable and produce collagen I, collagen III, and tenacin-C[156] showing ligament differentiation potential.[166]

Much of the tensile strength of ligament tissue comes from the structure of parallel collagen bundles. The idea of cell sheets for tissue engineering neglects this important design consideration, so the organization of the ECM may be different from that in natural tissue. A biodegradable oriented scaffold, such as an aligned electrospun

mesh may provide the guidance the cells and their ECM need to produce this aligned structure.

Cells can attach to ECM proteins on a scaffold–either present in natural biomaterials or after proteins from the cell growth media are adsorbed onto a synthetic surface –through integrins adhesion receptors. Integrins are trans-membrane proteins and the outer part recognizes a binding site on ECM proteins. On the inside of the cell, the integrins attach to the actin filaments, and the organization of the actin depends on the mechanical properties of the scaffold, by increasing organization with increased mechanical properties.

In 1945, the phenomenon of contact guidance was first discovered when cells were found to align with fibrin.[167] This behavior has since been observed with several types of cells (macrophages, fibroblasts, neurons) on many surfaces including metals, silicones, and polymethylmethacrylates[168] indicating that this is a generalized cell phenomenon. Oriented cells will also deposit oriented ECM.[129,130,169]

Studies performed on microgrooved surfaces have given insight on contact guidance. Groove width and depth have been shown to affect cell behavior. With equal width grooves between 2 and 10 μm, fibroblasts orientation was found to increase with decreased groove spacing.[170,171] The time required for fibroblasts to orient was also decreased on a 1 μm repeating groove structure as compared to other conditions,[172] indicating that smaller features have more effect on cell alignment. In a study on axon behavior, nanoscale grooves were shown to orient cells, but 100 nm surface features were too small for axons to sense, while they were guided by structures of 200 nm and larger.[173,174] The ideal feature size for ligament tissue engineering cells (MSC or ligament fibroblasts) may be able to be optimized for design of grafts.

Although fibrous meshes differ from grooved surfaces in several respects, they have also been shown to induce contact guidance. For these meshes, the fibers are round, rather than the straight walls on the grooved surfaces. Electrospun meshes are also a three-dimensional scaffold, where the orientation of the fibers may vary throughout the mesh. The thin fibers in electrospun meshes may be able to be deformed by cells. The

fiber diameter and alignment of the meshes, which control cell attachment and spreading, can be controlled by varying polymer concentration, molecular weight, and rotation speed of the collection drum.

Although electrospun meshes are a more complex system than the simple repeating groove structures, Lee et al found higher collagen expression from human ligament fibroblasts cultured on aligned fibers than those cultured on randomly oriented meshes.[175] Bashur et al found that NIH 3T3 fibroblasts cells adhered to and proliferated well on all PLGA meshed formed with varying fiber diameters (0.14 – 3.6 μm) and degrees of fiber orientation (32-60^{o}). Cells were able to align with the fibers of the mesh with increasing fiber diameter and increasing fiber orientation, indicating that with proper design considerations, electrospun meshes may be suitable for tissue engineered ligament scaffolds.[176] In another study by Bashur et al, rat bone marrow stromal cells express higher levels of ligament proteins with smaller fiber diameter PEUUR meshes, and there is a higher degree of alignment and elongation of cells with more alignment in the mesh fibers,[149] indicating that each scaffold system has to be optimized before application.

To further probe the use of electrospun mesh as a tissue engineered ligament graft, an experiment was designed comparing two methods for fabrication of a tissue engineered ligament graft, using only the ECM that cells produce to seal layers of electrospun mesh. The electrospun mesh was composed of poly(ester-urethane urea) (PEUUR), an elastomeric biomaterial that is capable of undergoing repetitive stretch in vitro, so may be able to be applied as a ligament tissue engineered scaffold. A cylindrical construct was fabricated using a rolling method to produce a scaffold with multiple layers of electrospun mesh with cells in-between these layers. The total culture time was 6 weeks for both fabrication methods, but the time before rolling varied. In the first method, cells were seeded onto the mesh and then cultured for four weeks. The mesh was then rolled to create a cylindrical structure, and then cultured for 2 more weeks. In the second fabrication method cells were cultured on the mesh for 2 weeks prior to rolling, and then four weeks as a cylindrical construct. The construct mechanical

properties and protein deposition of the two fabrication methods were compared. It was hypothesized that the method with longer culture time after rolling would produce a stronger graft.

4.2 Materials and Methods

4.2.1 Construct Fabrication and Initial Evaluation

Meshes were treated with DMEM containing 40% FBS overnight. The following day, meshes were rinsed with PBS and cells were seeded at 10,000 cell/cm^2 on to meshes which were anchored to the dishes using magnets The meshes were cultured in DMEM supplemented with 10% FBS, 1% PSA (10 U/mL penicillin, 10 g/L streptomycin, and 10 g/L amphotericin, Mediatech), and 1ng/ml TGF-β1 (Sigma) for 2 or 4 weeks. To fabricate cylindrical constructs, meshes were wrapped around 3 mm glass rods so that the electrospun mesh fibers were aligned circumferentially and cells faced outward. The rods were sterilized by autoclaving. After forming cylindrical constructs, specimens were cultured in DMEM containing 10% FBS, 1% PSA, 1ng/ml TGF-β1, and 50 μg/mg ascorbic acid for either 2 or 4 weeks depending on prior treatment for a total culture time of 6 weeks. In experiment 1, cells were cultured on the mesh for 4 weeks prior to rolling, and then 2 weeks after. For experiment 2, cells were cultured for 2 weeks before fabrication of a cylindrical construct, and then 4 weeks after.

4.2.2 Mechanical Property Assessment

The mechanical properties of the constructs were measured following 6 weeks of culture. For mechanical property assessments, 3-5 mm ring segments were cut using surgical scissors from constructs that had been immersed in media overnight. Circumferential mechanical tests were performed using a modification of the technique validated in Johnson et al.[91] Calipers were used to measure the dimensions of each construct segment. Each ring was then mounted onto an Instron 3342 equipped with a 10 N load cell using custom brackets.[137] The ring segments were exposed to uniaxial strain

at a rate of 6 mm/min until failure. Applied stress was calculated from the measured force by approximating the area of force application as two rectangles, each with sides equal to the width and wall thickness of the ring. The gauge length, l_g, was taken as the inner diameter, D_v, of the unstretched ring plus the wall thickness, h_v. The incremental or tangential modulus, E, of each sample was defined as the slope of the resulting stress–strain curve at a reference stress of 20 kPa to mimic the circumferential stress experienced by vessels under physiological pressures (~0.5 $P_{avg} D_v / h_v$).[152] The ultimate tensile strength (UTS) of the samples was defined as the maximum stress applied prior to failure.

4.2.3 Construct Analyses

After 6 weeks total culture time, the static and dynamic constructs were harvested for biochemical and mechanical analyses. Each construct was cut into 5 ring segments, each ~3-5 mm in length. The two end-segments were discarded. One segment per construct was allocated for mechanical testing. The remaining sections were immersed in formalin overnight, after which they were allocated for histological or biochemical assays. Mechanical testing was performed as described above. Details of the mechanical and histological analyses are given in the following sections.

4.2.4 Biochemical Analyses

Samples for biochemical analyses were transferred to 2 mL screw-cap microfuge tubes containing 1.5 ml of lysis buffer (PBS containing 1% Triton X-100, 0.5% SDS, and 100 µg/mL PMSF) and 1 mL of 3.2 mm stainless steel beads. Each sample segment was homogenized at 4800 rpm in a Bead-Beater homogenizer (Biospec, Bartlesville) in 10 s cycles with 1 min intermediate cooling on ice. Each sample was analyzed for collagen I(α1) (COL1A1, clone D-13), collagen III(α1) (COL3A1; clone S-17), and GAPDH (clone V-18) via competitive ELISA. In brief, peptide corresponding to the immunogen for each antibody were obtained from Santa Cruz Biotechnology (SCBT) and used to coat EIA plates at either 500 ng (collagen III peptides) or 2000 ng (collagen

I and GAPDH peptides) per well, after which the wells were blocked with BSA. At the time of analysis, samples were incubated with primary antibody for 1h, after which the mixtures were applied to the coated plates for 1 h. Standards were prepared by similarly incubating primary antibody with varying levels of immunogen peptide for 1 h, followed by application to coated plates. For both samples and standards, bound primary antibody was detected using appropriate HRP-conjugated secondary antibody, followed by application of 2,2'-azino-bis(3-ethylbenzthiazoline-6-sulphonic acid) (Sigma) and monitoring of absorbance at 410 nm.

4.2.5 Histological Analyses

Histological sections were fixed in formalin overnight at 4 °C, embedded in OCT media, and cut into 10 μm sections. ECM deposition and cell phenotype were analyzed in 2 sections per sample using standard immunohistochemical technique. In brief, rehydrated sections were blocked by 30 min exposure to Terminator (Biocare Medical). Primary antibodies for collagen type I (Rockland Immunochemicals, Gilbertsville), and collagen type III (Rockland Immunochemicals) were diluted in PBS containing 3% BSA and 0.5% Tween 20 and for 1 h at room temperature. Bound primary antibody was detected by using an appropriate HRP-conjugated secondary antibody (Jackson Immunoresearch) followed by application of the chromogen 3,3’-Diaminobenzidine (DAB; SCBT) Sections were then dehydrated with graded alcohol followed by xylene, and then mounted using polymount (Polysciences). Stained sections were imaged using an Axiovert microscope (Zeiss).

4.2.6 Statistical Analyses

Data are reported as mean ± standard error of the mean. Comparison of sample means was performed by one-way ANOVA, $p < 0.05$.

4.3 Results and Discussion

Cylindrical mesh scaffolds were produced by rolling a PEUUR electrospun mesh pre-seeded with 10T1/2 mouse mesenchymal cells, around a mandrel and securing the ends with ties. After either two or four weeks in culture, this process resulted in multiple layers of electrospun mesh secured by ECM produced by the cells. The ECM was found between and throughout the layers of the mesh. After 6 weeks total culture time, mechanical testing was performed followed by the completion of biochemical and histological analysis to determine the feasibility of using this system as a TE ligament graft.

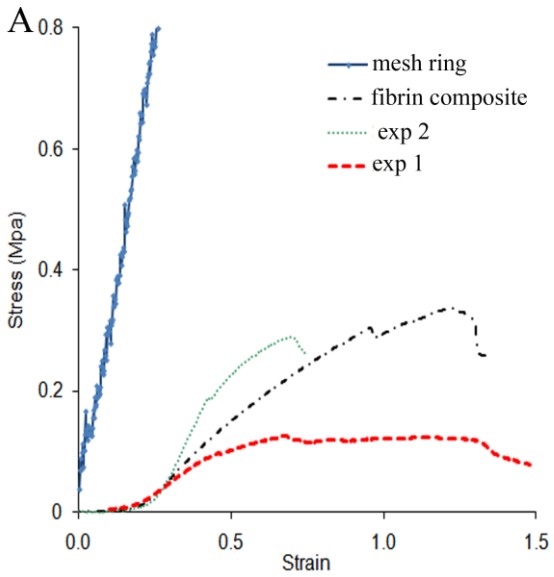

Figure 14: ECM-mesh, fibrin-mesh, and PEUUR electrospun mesh mechanical responses. (A) Compares a representative circumferential stress-strain response for the two fabrication methods. Experiment 1 had a 2 week culture time after rolling while experiment 2 had 4 weeks of culture after rolling. These are compared to the mechanical properties of a pure PEUUR electrospun mesh ring and a fibrin electrospun-mesh composite, adapted from McMahon et al[177].

Figure 14- part A shows the typical shape of a stress-strain curve from the two culture methods compared with a purely electrospun mesh ring segment. Single component scaffolds are generally unable to mimic the non-linear stress-strain behavior characteristics seen in native ligament. This is seen in the linear behavior of the mesh

ring. The fibrin-electrospun mesh composite was able to mimic the behavior of native ligaments, but lost much of the tensile strength associated with the pure mesh.[177] The construct labeled experiment 1 retains this biphasic stress-strain response, but 2 weeks of culture after rolling doesn't allow sufficient bonding time for the cells to produce strong and integrated ECM. The construct produced in experiment 2 shows the necessary behavior but retains much of the tensile modulus from the purely electrospun mesh (~1 MPa). This can be explained by the increased culture time following cylindrical construct fabrication, which allowed the cells to deposit more ECM, but also because the cells had additional time to remodel this ECM into a more ideal network. The UTS of both of the experimental formulations was lower than that of the fibrin-electrospun mesh composite, but may be improved with additional culture time.

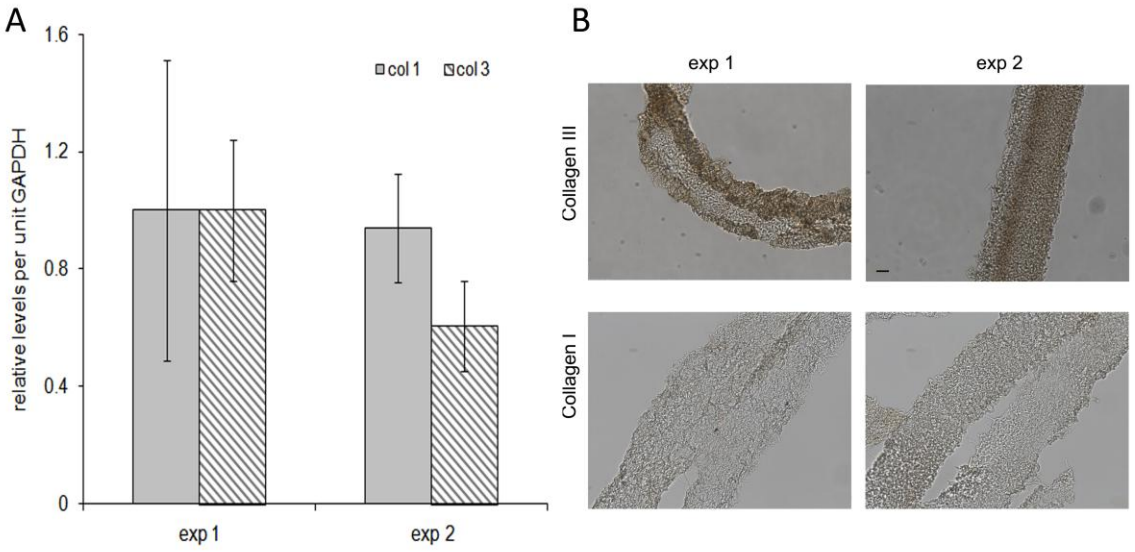

Figure 15: Immunostaining and biochemical comparison of fabrication methods (A) ELISA results for collagen I (col I) and collagen III (col 3) normalized to housekeeping protein GAPDH. (B) Representative images of transverse sections through composite constructs from both fabrication methods following immunostaining for collagen I and collagen III.

Both collagen I and collagen III production were slightly lower with longer culture after rolling, although these differences weren't significant (**Figure**

15- part A). This indicates that it may not be the about of ECM produced, but the arrangement of this ECM which is causing the increased mechanical properties exhibited by the ECM-mesh composites with longer culture time after rolling into a cylindrical construct. ECM remodeling is a continuous process in the body. Remodeling, common during wound healing, results in increased tensile strength, and can occur months to even years after injury. [178]

Cumulatively, the present results indicate that ECM-electrospun mesh composites warrant further investigation for ligament tissue engineering. Further studies will focus on increasing the cell infiltration through the mesh using a pressure difference [179] to pull the cells into the scaffold. This would make the process more clinically viable. Also, the expression of ECM components and phenotype markers has been shown to increase with stretch,[166] so future studies will incorporate mechanical conditioning.

CHAPTER V
INORGANIC-ORGANIC HYBRID SCAFFOLD FOR OSTEOCHONDRAL REGENERATION*

5.1 Introduction

The cruciate ligaments of the human knee withstand a variety of tensile and torsional forces during the course of normal daily routine and athletic activity. Damage can result in pain, joint instability and dysfunction, and eventual degenerative joint disease.[180] As such, approximately 150,000 surgical procedures are performed to treat injured anterior cruciate ligaments (ACLs) each year in the United States alone.[2] Currently, autologous tissue is the preferred graft material for ACL reconstruction.[181] However, the limited supply of autologous tissue suitable for grafting and the risk of donor site morbidity complicate the use of autologous grafts.[182] Tissue engineering is an alternative approach for ligament repair that may avoid many of limitations associated with autografts.

Although rapid progress has been achieved in ligament tissue engineering over the past decade, engineered ligaments have, thus far, generally failed to achieve mechanical properties sufficiently similar to their native counterparts to serve as viable grafts.[183] In addition, these engineered tissues usually lack the osteochondral interface critical to the appropriate transfer of load between ligament and bone.[183] Since graft failure frequently results from poor integration of the replacement tissue with associated bone,[184] the ability to regenerate the bone-ligament osteochondral interface would be advantageous in ligament reconstruction.

In orthopaedic tissue engineering, interfaces between tissues have a distinct role in the proper load transfer, making them crucial to tissue function.[185] These interfaces usually have physical and chemical properties differing from the tissues they connect. Failure to incorporate this tissue-to-tissue interface has been reported to compromise graft stability and long-term clinical outcome of ligament reconstructions.[185-187] For ligament or tendon tissue, the transition from bone occurs in three distinct regions: ligament, fibrocartilage, and bone. The fibrocartilage is further divided into calcified and non-calcified zones.[188] Thus, a scaffold which promotes a spatially-regulated transition in cell behavior from osteoblast-like to chondrocyte-like would be desirable for osteochondral regeneration.[189] For instance, a recent osteochondral tissue engineering study employed a scaffold containing a spatial gradient in levels of a retrovirus encoding for Runx2, an osteogenic transcription factor.[190] This design induced a spatially-graded transdifferentiation of associated dermal fibroblasts into osteoblast-like cells. Similarly, an extensive body of literature indicates that appropriately tailoring scaffold inorganic composition (hydroxyapatite and bioactive glass) can enhance its osteoconductivity.[191-194] Recently, silica-calcium phosphate composite scaffolds were shown to induce increasing osteoblast alkaline phosphatase activity[195] and osteocalcin expression[196] with increasing silica (decreasing calcium phosphate) content. Another work demonstrated elevated alkaline phosphatase activity in osteoblasts cultured on gelatin scaffolds of increasing siloxane content.[197]

We employed hydrogels composed of varying ratios of poly(ethylene glycol) (PEG) to star poly(dimethylsiloxane) ($PDMS_{star}$). PEG was selected for the organic component since spatial gradients can readily be fabricated in hydrogels prepared from diacrylate-derivatized PEG due to its photoactivity. For instance, PEG hydrogels with a continuous linear material property gradient can be generated by simple adaptation of the equipment normally used to make gradient polyacrylamide gels for electrophoresis.[198] More complex spatial gradients or patterns can be fabricated using photolithographic techniques[199-201] PDMS was chosen over other polysiloxanes due to its known biocompatibility and its widespread use in biomedical applications[202] In addition,

a star conformation of PDMS was selected over a linear form in order to reduce potential phase separation between the hydrophobic PDMS and hydrophilic PEG prior to hydrogel polymerization.[203]

In the present study, rat calvarial osteoblasts were encapsulated in PEG gels of varying $PDMS_{star}$ content, and the resulting modulation of cell behavior was examined. In assessing cell response, biochemical and histological analyses were conducted for extracellular matrix (ECM) components associated with mature bone (collagen type I, osteocalcin, and calcium phosphate (CaP)) and fibrocartilage (collagen types I and II as well as chondroitin sulfate proteoglycan (CSPG)).[188] To gain insight into the signaling underlying observed cell responses, immunostaining for the chondrogenic transcription factor sox9[204] was also performed.

5.2 Materials and Methods

5.2.1 Synthesis of methacrylate-derivatized $PDMS_{star}$ ($PDMS_{star}$-MA)

Methacrylate-derivatized star PDMS ($PDMS_{star}$ -MA) was prepared via a two step synthetic strategy per a modification of the methodology validated in Grunlan et al.[205] First, silane-terminated $PDMS_{star}$ ($PDMS_{star}$ -SiH) was prepared by the acid-catalyzed equilibration of octamethylcyclotetrasiloxane with tetrakis(dimethylsiloxane)silane. The desired $PDMS_{star}$ Mw of ~14 kDa was achieved by appropriately setting the ratio of these two components.[205] Briefly, octamethylcyclotetrasiloxane (30 g, 0.10 mol) and tetrakis(dimethylsiloxane)silane (0.5 g, 1.5 mmol) were combined in a 100 mL round bottom flask and purged with N_2. Triflic acid (15 μL) was then added and the reaction was allowed to stir for 1 h at 90°C. After cooling, the pH was neutralized by combining with $MgCO_3$ (0.5 g) and dichloromethane (DCM, 20 mL) and stirring for 2 h. After filtration through a pad of Celite, the volatiles were removed under reduced pressure. In this way, $PDMS_{star}$-SiH was obtained (26.3 g, 86% yield) as a colorless liquid and subsequently characterized by ^{1}H NMR, ^{13}C NMR, IR, and gel permeation chromatography (GPC).

The silane terminal groups of $PDMS_{star}$-SiH were then converted into photosensitive moieties by the hydrosilylation reaction of $PDMS_{star}$-SiH and allyl methacrylate. 25 Briefly, $PDMS_{star}$-SiH (6 g, 0.72 mmol) was combined with 10 mL of dry toluene in a 100 mL round bottom flask and purged with N_2. After Karstedt's catalyst (Pt-divinyltetramethyldisiloxane complex in xylene, 2% Pt; 15 lL) was added, the reaction was heated under constant stirring to 45°C. Allyl methacrylate (0.39 mL, 2.9 mmol) was added to this solution via an addition funnel over 15 min, after which the reaction was heated to 90°C and stirred overnight. Completion of the reaction was confirmed by the disappearance of the Si−H (~2100 cm^{-1}) absorbance in the IR spectrum. The reaction mixture was decolorized by refluxing with activated carbon for 12 h. After filtration, the volatile side products were removed under reduced pressure. In this way, methacrylate-derivatized $PDMS_{star}$ ($PDMS_{star}$-MA) was obtained (5.23 g, 82% yield) and subsequently characterized by ^{1}H NMR.

5.2.2 Preparation of Diacrylate-Terminated PEG

Photosensitive acrylate groups were introduced to the terminal ends of linear PEG (MW ~3.4 kDa, Sigma) per established protocols.[200] Briefly, PEG (10 g, 3.3 mmol) and dry DCM (50 mL) were combined in a 100 mL round bottom flask and purged with N_2. Triethylamine (0.96 mL, 6.6 mmol) was added slowly to the solution followed by the dropwise addition of acryloyl chloride (1.08 mL, 13.2 mmol). The reaction mixture was allowed to stir at room temperature overnight. Removal of HCl was accomplished by washing the mixture with 2M K_2CO_3 and separating into aqueous and organic phases. The organic (DCM) phase was then dried with anhydrous $MgSO_4$, and diacrylate-derivatized PEG (PEG-DA) was precipitated in diethyl ether and dried under vacuum. In this way, PEG-DA was obtained and subsequently characterized by ^{1}H NMR.

5.2.3 Synthesis of Acrylate-Derivatized Cell Adhesion Ligand

Cell adhesion peptide RGDS (American Peptide) was reacted with acryloyl-PEG-N-hydroxysuccinimide (ACRL-PEG-NHS, Mw ~3.4 kDa, Nektar) at a 1:1 molar

ratio for 2 h in 50 mM sodium bicarbonate buffer, pH 8.5. 19,20 The product (ACRL-PEG-RGDS) was purified by dialysis, lyophilized, and stored at -20^{o}C until use.

5.2.4 Hydrogel Fabrication

Three distinct hydrogel precursor solutions were prepared by dissolving desired levels of $PDMS_{star}$-MA and PEG-DA in HEPES buffered saline (HBS; 10 mM HEPES, 150 mM NaCl, pH 7.4). Each solution contained 10 weight percent (wt %) total polymer comprised of one of the following three wt ratios of $PDMS_{star}$-MA to PEG-DA: 0:100, 1:99, and 5:95. Ten microliters of photoinitiator consisting of a 30 wt % solution of 2,2-dimethyl-2-phenyl-acetophenone in N-vinylpyrrolidone was added per milliliter of precursor solution. The resulting solutions were mixed by vortex and then filtered (0.22 μm PES membrane, Millipore) immediately prior to being pipetted into 0.5-mmthick transparent rectangular molds. In addition to performing a sterilization function, the filtration process served to create a fine and stable dispersion of hydrophobic $PDMS_{star}$-MA within the aqueous PEG-DA solution. The precursor solutions were polymerized by 2 min exposure to longwave UV light (Spectroline, ~6 mW/cm^2, 365 nm).

5.2.5 Hydrogel Composition

To verify the incorporation of varying levels of $PDMS_{star}$ into the fabricated hydrogels, compositional analysis was performed using a Kratos Axis Ultra X-ray photoelectron spectrometer (XPS) with a monochromatized Mg Ka source. Swollen hydrogels were transferred to dIH2O for 24 h and then dried under vacuum. The dried gel discs were then placed onto steel gravity mounts and loaded into the XPS. Elemental atomic percent compositions were obtained from survey spectra, which were performed from 0 to 1100 eV. High-resolution analyses with pass energies of 40 eV were performed at a take-off angle of 90^{o}. The binding energies were referenced to C^{1s} peak at 285.0 eV. The raw data was quantified and analyzed using XPS Peak Processing software.[206]

5.2.6 Contact Angle and Protein Adsorption

The dependence of gel surface hydrophilicity and protein adsorption on increased $PDMS_{star}$ content was evaluated. Static contact angle measurements were performed on swollen $PDMS_{star}$ -PEG hydrogels using a CAM-200(KSV Instruments) contact angle measurement system equipped with an autodispenser, video camera, and dropshape analysis software. Briefly, 5 μL of dIH2O was dispensed onto each hydrogel surface, and the angle of the water droplet relative to the surface was monitored for a period of 2 min. Five separate measurements were performed for each hydrogel formulation.

For protein adsorption analyses, four 6-mm diameter samples were harvested from swollen hydrogels of each formulation. These samples were exposed to a 50 μg/mL solution of AlexaFluor 488-labeled fibronectin in PBS. Fibronectin adsorption was selected for characterization based on previous bone tissue engineering studies.[207,208] Following 1 h at room temperature, the protein solutions were removed and exchanged with PBS. One hour and 12 h after removal of the protein solution, the fluorescence of the hydrogel surfaces was monitored using a Zeiss Axiovert 200 microscope and separately using a microplate reader at ex/em 488/532. Prior to each time point measurement, the PBS was removed and exchanged with fresh PBS. A fibronectin standard curve was used to convert each fluorescence signal to a protein concentration.

5.2.7 Hydrogel Swelling

To characterize equilibrium swelling, 8-mm diameter samples were cored from each PEG-DA hydrogel immediately following polymerization and weighed. The samples were then transferred to HBS supplemented with 0.05 wt % sodium azide (HBS-azide). After 24 h, samples were blotted and weighed. The swollen gels were then dried *in vacuo* and their dry weight recorded. As PEG-DA hydrogels are primarily water, the increase in weight with swelling can be directly related to the increase in gel volume (V) with swelling, i.e., $S = \left(\frac{V_{swollen}}{V_{initial}}\right) \sim \left(\frac{weight_{swollen}}{weight_{initial}}\right)$. S values were found to be 1.10 ± 0.01, 1.07 ± 0.01, and 1.11 ± 0.01 for the 0:100, 1:99, and 5:95 gels, respectively.

These ratios were used to calculate the amount of cells and ACRL-PEG-RGDS to be added to each hydrogel precursor solution so as to ensure the desired postswelling cell density and RGDS concentration. The dry weight measures were used to calculate the swelling ratio for each formulation: R = (swollen weight/dry weight). This ratio served as an indicator of gel crosslink density.

5.2.8 Hydrogel Mesh Size

PEG-DA hydrogel mesh structure cannot be visualized using techniques such as conventional scanning electron microscopy (SEM). [209] Thus, a variety of methods to estimate PEG-DA hydrogel mesh size have been developed, including correlations linking measurable quantities, such as equilibrium hydrogel swelling and PEG-DA M_n, to mesh size.[210,211] Although these correlations yield reasonable mesh size estimates for homopolymer hydrogels, [210,211] these correlations cannot readily be applied to $PDMS_{star}$ –PEG hybrid hydrogels. Thus, in this study, hydrogel mesh size was characterized via dextran diffusion based on an adaptation of the methodology of Watkins et al. [212]

A series of $PDMS_{star}$ -PEG hydrogels were prepared, each containing 1 μM ACRL-PEG-RGDS postswelling. These gels were allowed to swell overnight at 37°C in HBS-azide, after which 8 mm discs were cored from each sample. FITC-labeled dextran (70 kDa, Sigma) was dissolved at 0.05 mg/mL in HBS-azide and added at 1 mL per hydrogel disc. Dextran was then allowed to diffuse into the hydrogels for 24 h at 37°C. Each gel disc was gently blotted and transferred to 1 mL fresh HBS-azide. Dextran that had penetrated into the hydrogels was then permitted to diffuse out into the surrounding solution at 37°C. After 24 h, the fluorescence of the HBS-azide solution surrounding each disc was measured at ex/em 488/532. Dextran standard curves were used to convert each fluorescence signal to microgram dextran. For each gel sample, these dextran readings were divided by gel weight to yield a quantitative indicator of hydrogel permissivity (C). These permissivity measures were used to estimate the relative mesh size (n) of each hydrogel (x) as follows:

$$\xi_x \sim \frac{C_x}{C_{0:100\,PDMS-PEG}}.$$

5.2.9 Hydrogel Mechanical Properties

$PDMS_{star}$ -PEG hydrogels were prepared containing 1 μM ACRL-PEG-RGDS postswelling. Three 8-mm discs were cored from each swollen gel and mechanically tested under unconstrained compression at room temperature using an Instron 3342. Following application of a 0.01 N preload, each hydrogel was subjected to 10 μm cyclic compression (~1% cyclic strain) at 1 Hz. The compressive modulus of each hydrogel was extracted from the resulting stress-strain data.

5.2.10 Cell Expansion

Cryopreserved rat calvarial osteoblasts (Dominion Pharmakine) were thawed and expanded at 37°C/5% CO_2 in Dulbecco's Modified Eagles' Media (DMEM, Hyclone) supplemented with 10% fetal bovine serum (FBS), and 100 mU/mL penicillin and 100 mg/L streptomycin (Hyclone).

5.2.11 Cell Encapsulation

Osteoblasts at passage 6 were harvested and combined. Precursor solutions containing 10 wt % total polymer were prepared by dissolving $PDMS_{star}$ -MA and PEG-DA at ratios of 0:100, 1:99, and 5:95 in HBS followed by photoinitiator. These wt ratios will be used to refer to the various hydrogel formulations throughout the remainder of the text. ACRL-PEG-RGDS was added to each precursor solution to achieve 1 mM RGDS post-swelling. Each precursor solution was sterile-filtered, immediately after which osteoblasts were added at a postswelling density of ~3 × 10^6 cells/mL. The hydrogel slabs were transferred to Omnitrays (Nunc) fitted with four sterile polycarbonate bars to simultaneously prevent gel flotation and prevent gel contact with the tray bottom. Gels were maintained at 37°C/ 5% CO2 in DMEM supplemented with

10% FBS and 100 mU/mL penicillin and 100 mg/L streptomycin. Media was changed every 2 days.

5.2.12 Day 3 Construct Analyses

Following 3 days of culture to allow for complete hydrogel equilibration, 8-mm diameter samples were collected to characterize the initial mechanical properties of the cell-laden gels. These measures were conducted as described earlier to assess the impact of cells on initial bulk-average hydrogel material properties (since hydrogel modulus, mesh size, and swelling are interdependent).[213]

5.2.13 Day 28 Construct Biochemical Analyses

After 28 days total culture time, a series of 8-mm samples were collected from each hydrogel formulation for biochemical and histological analyses. Samples harvested for biochemical analyses were weighed, flash-frozen in liquid nitrogen, and stored at -80 ^{o}C.

5.2.14 DNA and Total Collagen Biochemical Analyses

Hydrogel samples were digested for 72 h at 37^{o}C in 1 mL of 0.12M NaOH per 0.2 g hydrogel wet weight. Aliquots of the NaOH hydrolyzed samples (n = 3–6 per formulation) were neutralized and their DNA content determined using the PicoGreen assay (Invitrogen).[92] DNA measures were translated to cell number using a conversion factor of 6.6 pg DNA per cell. Calf thymus DNA (Sigma) served as a standard.

Levels of hydroxyproline were quantified as an indirect measure of total collagen. NaOH digested hydrogels (n = 3–5 per formulation) were further hydrolyzed for 18 h at 110^{o}C in 6M HCl. The samples were then dried (Centrivap, Labconco) followed by resuspension in dIH2O and reaction with chloramine T and p-dimethylbenzaldehyde reagents.[214] Sample absorbance was read at 550 nm relative to that of l-4-hydroxyproline (Sigma). Total collagen content was estimated from measured hydroxyproline using the collagen type I conversion factor of 0.13 grams hydroxyproline

per gram collagen.[215] For each assay, the standards used were subjected to the same association with PEG-DA and $PDMS_{star}$ -MA and the same digestion conditions as the samples.

5.2.15 Calcium and Alkaline Phosphatase Analyses

Hydrogels (n = 2 per formulation) were transferred to 2 mL screw-cap microfuge tubes containing 1 mL of lysis buffer from the EnzoLyte FDP Alkaline Phosphatase assaykit and 1 mL of 3.2 mm stainless steel beads. Each sample was homogenized at 4800 rpm in a Bead-Beater homogenizer (Biospec) in 10 s cycles with 1 min intermediate cooling on ice. Two hundred microliter aliquots of each sample homogenate were analyzed for alkaline phosphatase activity using EnzoLyte kit reagents. Total calcium was assessed from 5 lL aliquots of each sample homogenate using the Calcium CPC liquid color kit (Stanbio).

5.2.16 Day 28 Histological Analyses

To gain further understanding of the effects of hydrogel composition on the behavior of encapsulated cells, staining was conducted for ECM components associated with mature bone (collagen type I, osteocalcin, and CaP). Similarly, immunostaining for fibrocartilage-associated ECM components (collagen type I, collagen type II, and CSPG) and for chondrogenic transcription factor sox9 was carried out. Samples harvested for histological analyses were fixed with 10% formalin for 30 min, embedded in freezing media (Tissue-Tek), and cut into 35 μm sections.

5.2.17 Immunostaining

Immunostaining was conducted according to standard protocols. In brief, sections were blocked with peroxidase (Biocare Medical) for 30 min followed by Terminator (Biocare Medical) for 10 min. Primary antibody for osteocalcin [FL-95, Santa Crux Biotechnology (SCBT)], collagen type I (Rockland Immunochemicals), collagen type II (Rockland), CSPG (cs-56, SCBT), or sox9 (H-90, SCBT) was then

applied for 1 h following dilution in HBS. For the sox9 antibody, sections were permeabilized before antibody application with PBS containing 0.05% Triton-100X. For each antibody and hydrogel sample, 2–3 sections were stained. Bound primary antibody was detected by using AP-/HRP-conjugated secondary antibodies (Jackson Immunochemicals) followed by application of chromogen (LabVision).

5.2.18 Van Kossa Staining

To detect calcium deposits, sections were stained using a standard van Kossa staining kit (American MasterTech Scientific). In brief, rehydrated sections were rinsed with dIH2O, after which a 5% silver nitrate solution was applied. Sections were then exposed to full spectrum light in a humidified chamber for 45 min. After rinsing with dIH2O, sections were exposed to a 5% sodium thiosulfate for 2.5 min, briefly rinsed, and mounted.

5.2.19 Semiquantitative Histological Assessments

For intracellular transcription factor sox9, cell counts were conducted to semiquantitatively evaluate immunostaining results. In addition, as deposited ECM remained localized around the parent cells in each hydrogel formulation (**Figures 16 and 17)**, the relative ECM protein production among hydrogel formulations could also be evaluated by cell counts. For each stained section (containing ~250 cells), these semiquantitative analyses were conducted per established protocols.[216-220] In brief, staining intensity, d_i, was recorded for each cell, i, on a scale of 0–3, with 0 =‘‘no staining’’ and 3 = ‘‘highest staining intensity among all sections for that antibody’’. The cumulative staining intensity, d, for a given antibody in a particular section was calculated as: $d = (\Sigma\ d_i)/(\text{total cell number})$. The d value for all sections of a given hydrogel formulation were averaged to yield an overall sample average for each antibody. Immunostained samples were imaged using an Axiovert 200 microscope (Zeiss).

5.2.20 Statistical Analyses

Data are reported as mean ± standard deviation. Comparison of sample means was performed by ANOVA and Tukey's post hoc test (SPSS software), $p < 0.05$.

5.3 Results and Discussion

Hydrogels with a 0:100, 1:99, or 5:95 wt ratio of $PDMS_{star}$ to PEG were prepared and their initial composition, mesh size, and mechanical properties characterized. Results from these characterization studies are summarized in **Table 3**. For each gel formulation, the mass percent of Si determined by XPS was consistent with the value predicted from the known M_n of both polymers and the wt ratio of $PDMS_{star}$-to-PEG in the precursor solution. These data support the successful incorporation of $PDMS_{star}$ into the hydrogel networks.

Table 3: Initial material properties of $PDMS_{star}$-PEG hybrid hydrogels

$PDMS_{star}$ to PEG Weight Ratio	Relative Mesh Size (ξ)	Modulus (kPa)	Mass Percent Si	
			Measured	Predicted
0:100	1.0 ± 0.1	167 ± 8	0.0	0.0
1:99	1.1 ± 0.1	142 ± 4	0.6	0.4
5:95	1.3 ± 0.1	142 ± 11	2.3	2.0

The equilibrium diffusion of dextran was used to evaluate the mesh size of the 1:99 and 5:95 gels relative to the 0:100 gels (i.e., relative to pure PEG hydrogels). Gel mesh size increased directionally with increasing $PDMS_{star}$ content (**Table 3**). In contrast, the compressive moduli of the 1:99 ($p = 0.018$) and 5:95 ($p = 0.015$) hydrogels were significantly lower than that of the 0:100 gel (**Table 3**). Cell presence did not significantly impact observed initial bulk modulus assessments (data not shown), as expected given the relatively low initial cell density employed (~$3x10^6$ cells/mL)[216] The trends in both modulus and relative mesh size were consistent with a reduced crosslink density with increasing $PDMS_{star}$ content, in agreement with the greater M_n of each $PDMS_{star}$ arm relative to PEG.[213]

Table 4: $PDMS_{star}$-PEG hydrophilicity and Protein Adsorption

$PDMS_{star}$ to PEG Weight Ratio	Contact Angle (°)		Fibronectin Adsorption (ng/cm^2)	
	1 min	2 min	1 h	2 h
0:100	38.8 ± 3.9	35.3 ± 4.9	48.9 ± 1.1	13.3 ± 2.3
1:99	34.2 ± 3.4	32.0 ± 2.9	36.6 ± 3.0	14.5 ± 3.1
5:95	37.0 ± 9.1	34.6 ± 8.5	33.0 ± 14.7	14.5 ± 3.1

Since scaffold hydrophilicity[221] and protein adsorption[191,208] have been demonstrated to significantly impact osteoblast behavior, the surface hydrophilicity of and fibronectin adsorption on each hydrogel was investigated. In agreement with the literature,[206,222] contact angle measures indicated that $PDMS_{star}$-PEG hybrid scaffolds maintained the hydrophilic character of pure PEG gels (**Table 4**). Similarly, the equilibrium (12 h) levels of fibronectin adsorption on the $PDMS_{star}$-containing gels were statistically indistinguishable from those on pure, "non-biofouling" PEG hydrogels (i.e., the 0:100 $PDMS_{star}$-PEG gels, **Table 4**).[223]

Net cell density and ECM synthesis were evaluated in each hydrogel formulation to probe the influence of $PDMS_{star}$ levels on osteoblast behavior. Based on DNA measures, the cell densities in the 0:100, 1:99, and 5:95 hydrogels at day 28 were 1.93 ± 0.11, 1.93 ± 0.25 and 2.15 ± 0.19 million cells per gram, respectively. These data indicate that the net cell proliferation and loss over the time course of the study was similar across hydrogels and consistent with previous tissue engineering studies using "non-degradable" PEG-DA gels.[224] In contrast, osteoblast total collagen production showed marked variations with hydrogel composition. Specifically, the total collagen levels in the 0:100 ($p = 0.049$) and 5:95 ($p = 0.006$) gels were approximately 2 times greater than in the 1:99 hydrogels (**Figure 16- part A**).

To gain further insight into the observed total collagen results, immunostaining was conducted for collagen type I (associated with mature bone and, to a lesser extent, with fibrocartilage) and for collagen type II (associated with fibrocartilage).[188] These histological analyses revealed a modulation of collagen types I and II with gel formulation. Collagen type II production was significantly higher in the 5:95 hydrogels relative to the 0:100 ($p = 0.032$) and 1:99 ($p = 0.019$) gels (**Figure 16- part B**). In

contrast, collagen type I expression appeared to decrease directionally with increasing hydrogel inorganic content, although this trend was not statistically significant (**Figure 16- part C**).

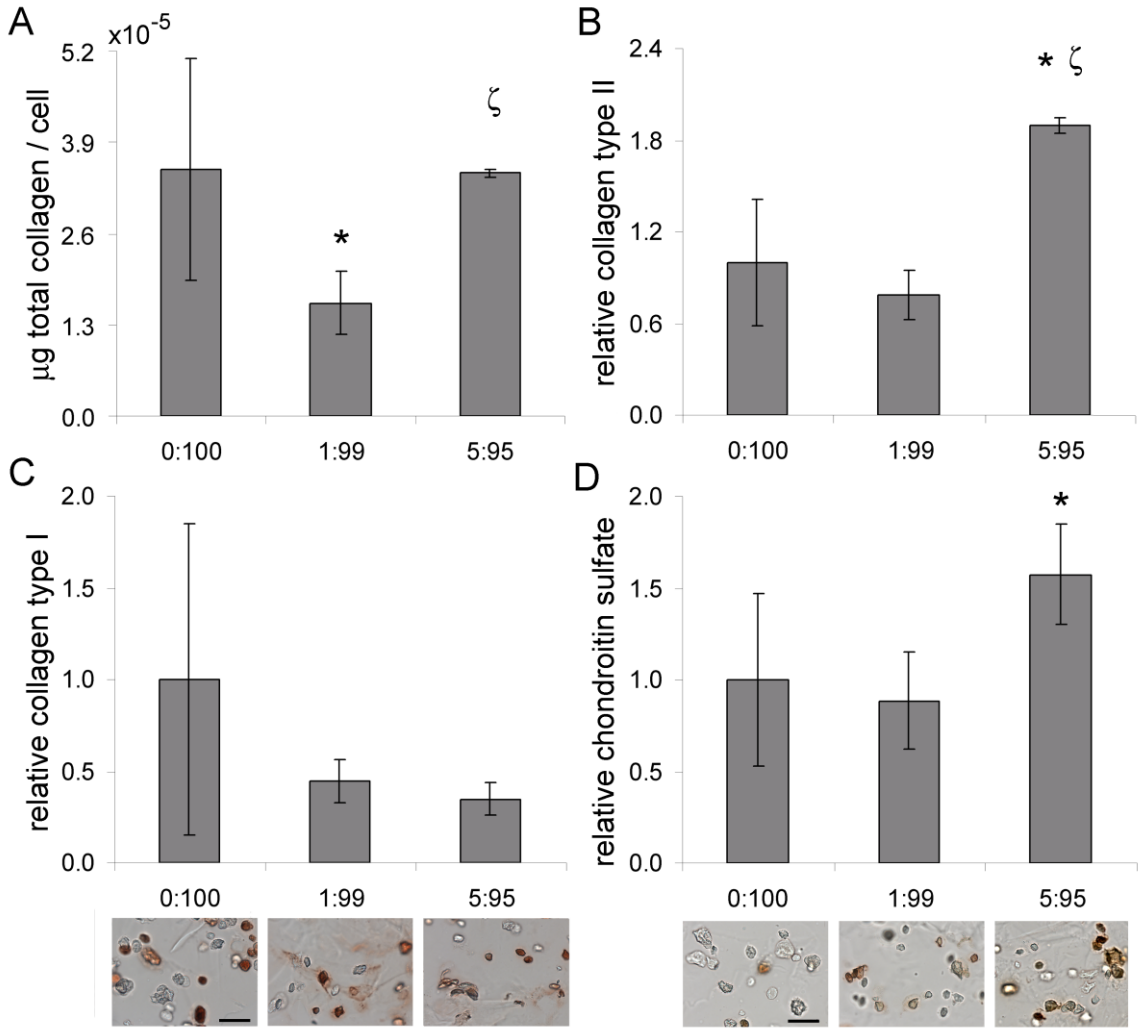

Figure 16: Relative expression of **(A)** total collagen, **(B)** collagen type II, **(C)** collagen type I, and **(D)** chondroitin sulfate across hydrogel formulations.*, significantly different from 0:100 gels; ζ, significantly different from 1:99 gels. Representative images of staining for collagen type I and chondroitin sulfate are shown below the respective graphs. Scale bars apply to each image in the series and equal 50 µm.

CSPG and sox9 (associated with fibrocartilage) as well as alkaline phosphatase, calcium deposits, and osteocalcin (mid-to-late term markers of bone tissue formation) were also assessed. CSPG levels were significantly higher in the 5:95 gels relative to the

0:100 hydrogels ($p = 0.037$, **Figure 16- part D**). In addition, sox9 expression increased with an increase in hydrogel inorganic content from 0:100 to 5:95 ($p = 0.011$, **Figure 17- part A**). Although no significant differences in alkaline phosphatase expression were noted among formulations (**Figure 17- part B**), van Kossa staining results revealed the levels of deposited calcium to be markedly higher in the 0:100 $PDMS_{star}$-PEG gels than in the 1:99 ($p < 0.001$) and 5:95 ($p < 0.001$) gels (**Figure 17- part C**). This decrease in calcium deposition with increasing hydrogel inorganic content was further reflected in the results from the CPC assay, which yielded 0.54 ± 0.13, 0.20 ± 0.14, and 0.18 ± 0.05 ng calcium per cell for the 0:100, 1:99, and 5:95 gels, respectively. Similarly, osteocalcin levels were reduced in the 5:95 gels relative to both the 0:100 ($p = 0.008$) and 1:99 ($p = 0.027$) hydrogels (**Figure 17- part D**).

In the present work, rat calvarial osteoblasts were encapsulated in a series of PEG-based hydrogels of increasing $PDMS_{star}$ content. Osteoblasts appeared to transdifferentiate into chondrocyte-like cells with increasing scaffold inorganic content, as indicated by increased chondroitin sulfate and collagen type II production and by upregulation of sox9. Furthermore, the synthesis of bone-like matrix (calcium deposits and osteocalcin) decreased with increasing $PDMS_{star}$ levels. Combined, the present results indicate that $PDMS_{star}$–PEG hybrid gels warrant further study as osteochondral regeneration matrices.

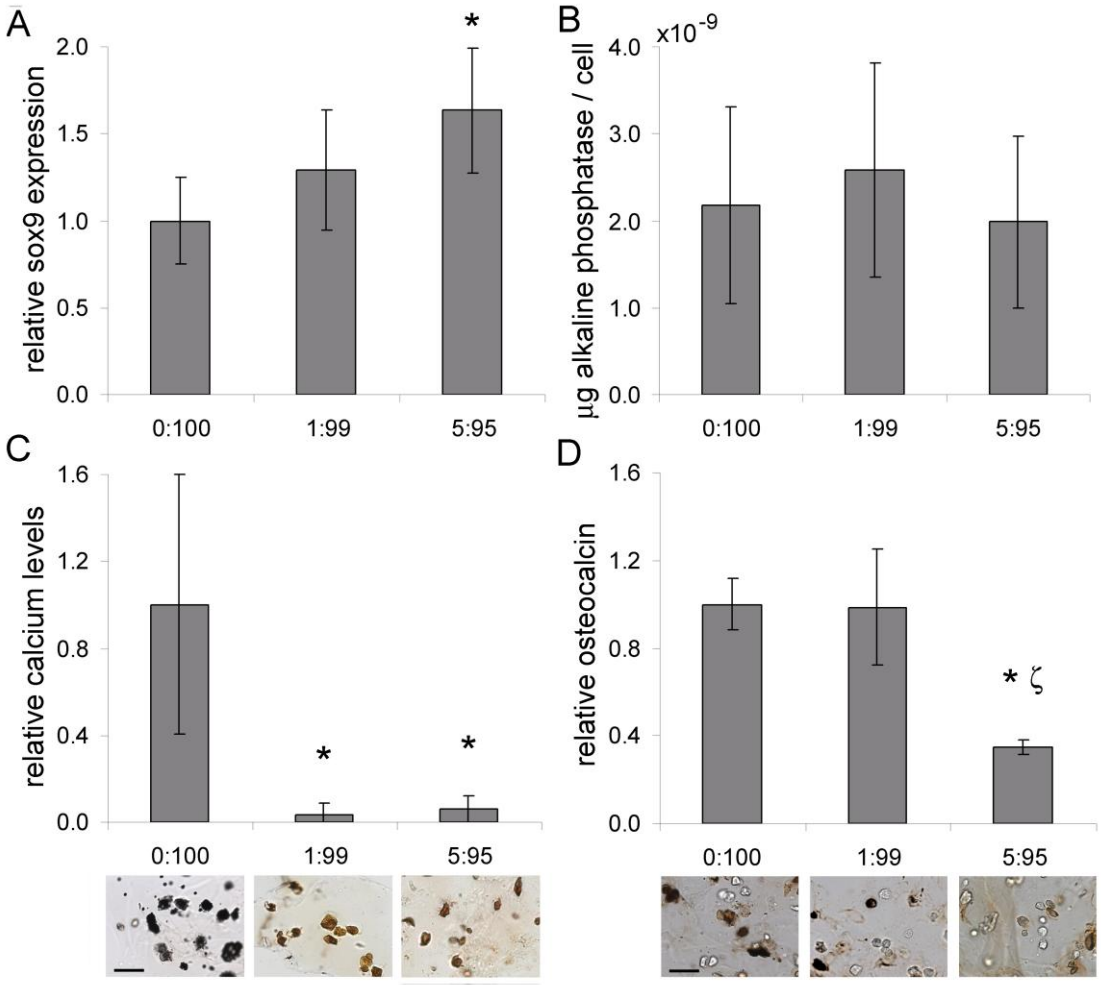

Figure 17 : Relative expression of **(A)** sox9, **(B)** alkaline phosphatase, **(C)** calcium, and **(D)** osteocalcin levels on hydrogel composition.*, significantly different from 0:100 gels; ζ, significantly different from 1:99 gels. Representative images of staining for collagen type I and chondroitin sulfate are shown below the respective graphs. Scale bars apply to each image in the series and equal 50 µm.

CHAPTER VI
CONCLUSIONS AND FUTURE WORK

Imagine a day where a patient will go to the hospital with an injury and leave totally cured by a procedure that not only fixes the problem but uses the patients own cells to do it. Tissue engineering is moving towards the day where shelf-life is no longer an issue as treatments could be produced *in situ.* For example, for the tissue engineered ligament graft, fibrin could be harvested from the patients blood and mesenchymal stem cells could be extracted from adipose tissue in the surgical suite, and combined with an electrospun mesh and growth factors to aid in differentiation, to generate a completely degradable graft. With time, those cells will differentiate into ligament fibroblasts and generate the ECM necessary to withstand the tensile forces as the mesh degrades away. These studies may be in their infancy, but with advances in tissue engineering, this could be a routine hospital visit within a few decades.

Many aspects of the treatment of knee joint damage were examined in this research. First, to overcome many of the limitations of total knee replacement, a novel TiNb alloy was investigated. This alloy is composed of biocompatible constituents, and was shown to be at least as biocompatible as pure Ti. The corrosion resistance was also high, similar to that of Ti and better than NiTi, so the behavior of TiNb would be expected to be similar to Ti when implanted. These promising results warrant further investigation into processing techniques like producing a porous TiNb.

Electrospun PEUUR meshes were explored, both as a composite scaffold with a hydrogel and alone, as a scaffold for ligament tissue engineering. In both studies, collagen I, collagen III, and elastin were deposited into the mesh by the mouse mesenchymal cells, indicating that the cells were producing the ECM proteins commonly found in ligament. Both of these fabrication methods produced the “toe-in” region commonly found in ligament tissue, and therefore better mimic native tissue than typical electrospun tubular scaffolds. The original mesh used had a tensile modulus of 1 MPa, which is much lower than native ligament, whose modulus ranges from 111-141

MPa.[105] Applying a similar technique to produce a construct using an electrospun mesh with higher tensile properties may generate a ligament graft with mechanical properties closer to those of native ligament. For example, this process could be used to produce a composite scaffold composed of a hydrogel and a stronger mesh, like the one produced by Huang et al. with a Young's modulus of 1.8 GPa.[155]

Optimizing the culture conditions for cell differentiation into ligament fibroblasts also needs to addressed before this method could be applied for *in vivo* ligament tissue engineering studies. In both electrospun mesh experiments, the main components of ligament ECM were produced, but growth factors could be applied to promote differentiation into ligament fibroblasts and the production of proper ECM. Future studies should also look at human mesenchymal stem cells to ensure they behave in a similar manner to the mouse cells used in the study. Finally, for a fully functional ligament tissue, the transition zone associated with the bony insertion ends of the ligaments must be recreated. An increase in organic content in the form of PDMS was shown to promote transdifferentiation of rat osteoblasts towards cartilage-like cells. Gradients in material properties of either the hydrogel or electrospun mesh could be utilized to promote differentiation of mesenchymal stem cells to recreate this transition region in ligament grafts. The gradient could either be produced in the hydrogel component or the electrospun component of the composite ligament graft.

Figure 18: Tissue engineered ligament graft with gradient to promote osteochondral interface regeneration by altering properties of mesh to direct MSC differentiation

Creating the gradient toward the ends of the electrospun component of the composite would simplify a procedure if this process ever were commercialized. A gradient can be produced by co-electrospinning two solutions onto a rotating drum. A charged guide is used to direct the fibers toward the drum and varying the offset of the

needles.[225] This can be utilized to alter mechanical properties, organic content, hydrophobicity, or growth factor concentration, in order to promote cell differentiation from ligament to fibrocartilage to bone and recreate this transition zone (**Figure 18**).

The benefits of scaffolds produced by electrospinning include their high porosity, high tensile strength, and ability to orient fibers to influence cell behavior. An oriented electrospun mesh can be applied as a scaffold to generate oriented tissues such as vascular tissue or nerve tissue in addition to ligament. Our lab is interested in pursuing a hydrogel-electrospun mesh composite, similar to the one developed for ligament tissue engineering as a vascular tissue engineering system.

A major limitation to the widespread use of electrospinning for tissue engineering applications is the inability of cells to infiltrate into the material. The porosity of electrospun meshes is very high, but the pore size is generally less than 10 μm so many groups have tried to increase cell infiltration by treating the meshes, producing meshes with larger pores[225], and processing meshes. These processing methods include electrospinning directly onto layers of cells[226] and using a vacuum to pull cells into the material.[179]

In an attempt to increase cell infiltration, a vacuum system similar to the one mentioned was used to pull cells into an elastomeric mesh for a preliminary vascular tissue engineering experiment. After one day in culture, a small sample was used to verify cell infiltration. Following two weeks in culture, a contractility test was successfully performed, indicating that the cells not only infiltrated the mesh, but were able to differentiate into smooth muscle like cells, form a network, and then contract with the addition of phenylephrine. With future ligament tissue engineering studies, this cell infiltration technique will be applied to ensure cells are dispersed throughout the scaffold and not just in between layers.

Figure 19 shows the gradient containing ligament graft as a treatment for a torn ACL. This graft contains adipose derived MSC who are directed to differentiate through the differences in organic content,[227] mechanical properties,[228`] the addition of chemical or biological factors[229] or a combination, which would be determined through

experimentation. The osteochondral interface present in natural ligament would be integrated into the bony ends of the graft, and the scaffold would degrade as the cells construct ECM to produce a healthy, functional ACL.

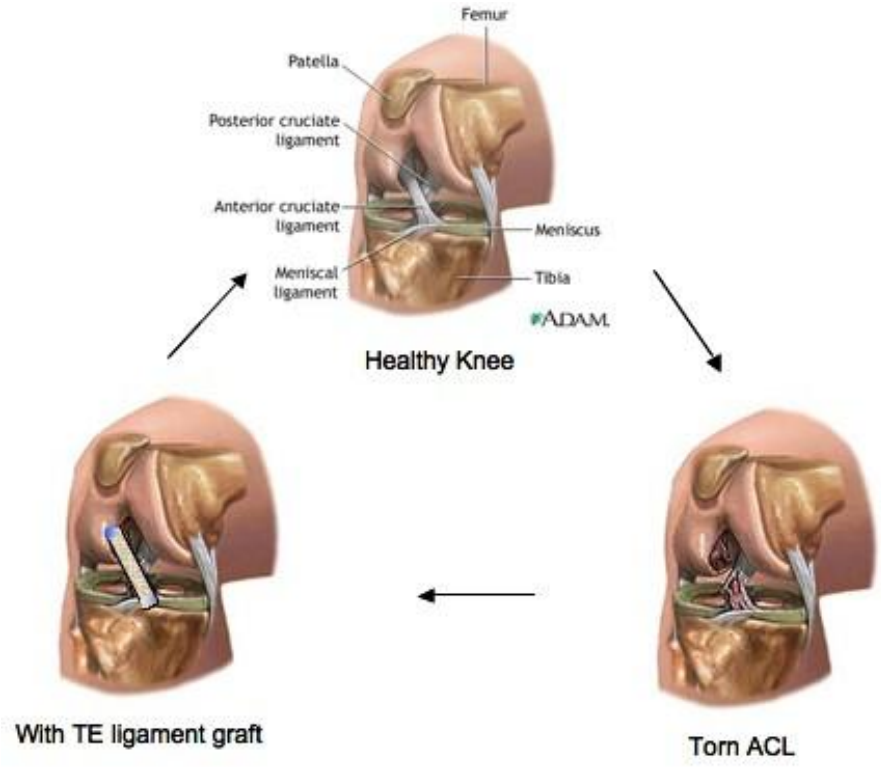

Figure 19: Process of treating a torn ACL with a TE ligament graft

Tissue engineering is a rapidly growing field with a great deal of potential to develop living substitutes for many tissues and organs. The form and function of defective or damaged body parts may be able to be replaced allowing for the regeneration of these tissues and the treatment or cure of many ailments and diseases. The introductory work in ligament and bone tissue engineering discussed may be able to be applied toward the development of future treatments of knee joint damage.

REFERENCES

1. Manner PA. Total knee arthroplasty: Pearls and pitfalls. AAOS Now. Rosemont, Illinois: American Academy of Orthopaedic Surgeons; 2008.

2. Cooper JA, Lu HH, Ko FK, Freeman JW, Laurencin CT. Fiber-based tissue-engineered scaffold for ligament replacement: design considerations and in vitro evaluation. Biomaterials 2005;26(13):1523-1532.

3. Amis AA, Dawkins GPC. Functional-anatomy of the anterior cruciate ligament - fiber bundle actions related to ligament replacements and injuries. Journal of Bone and Joint Surgery-British Volume 1991;73(2):260-267.

4. Bottoni CR, Liddell TR, Trainor TJ, Freccero DM, Lindell KK. Postoperative range of motion following anterior cruciate ligament reconstruction using autograft hamstrings - A prospective, randomized clinical trial of early versus delayed reconstructions. American Journal of Sports Medicine 2008;36(4):656-662.

5. Jomha NM, Borton DC, Clingeleffer AJ, Pinczewski LA. Long term osteoarthritic changes in anterior cruciate ligament reconstructed knees. Clinical Orthopaedics and Related Research 1999(358):188-193.

6. Buckwalter JA, Mankin HJ. Articular cartilage: Degeneration and osteoarthritis, repair, regeneration, and transplantation. Instructional Course Lectures 1998;47:487-504.

7. Surgeries and Procedures: Knee arthroscopy Volume 2010: A.D.A.M. Medical Illustration Team; 2001.

8. Miyasaka KC DD, Stone ML, Hirshman P. The incidence of knee ligament injuries in the general population. American Journey of Knee Surgery 1991;4:3-8.

9. Bruesch M, Holzach P. [Epidemiology, treatment and follow-up of acute ligamentous knee injuries in Alpine skiing]. Z Unfallchir Versicherungsmed 1993;Suppl 1:144-55.

10. Sgaglione NA, Delpizzo W, Fox JM, Friedman MJ. Arthroscopically assisted anterior cruciate ligament reconstruction with the pes anserine tendons - Comparison of Results in Acute and Chronic Ligament Deficiency. American Journal of Sports Medicine 1993;21(2):249-256.

11. Finsterbush A, Frankl U, Matan Y, Mann G. Secondary damage to the knee after isolated injury of the anterior cruciate ligament. Am J Sports Med 1990;18(5):475-479.

12. Marder RA, Raskind JR, Carroll M. Prospective evaluation of arthroscopically assisted anterior cruciate ligament reconstruction. Patellar tendon versus semitendinosus and gracilis tendons. Am J Sports Med 1991;19(5):478-484.

13. Aglietti P, Buzzi R, Zaccherotti G, De Biase P. Patellar tendon versus doubled semitendinosus and gracilis tendons for anterior cruciate ligament reconstruction. Am J Sports Med 1994;22(2):211-218.

14. Brown CH, Steiner ME, Carson EW. The use of hamstring tendons for anterior cruciate ligament reconstruction - technique and results. Clinics in Sports Medicine 1993;12(4):723-756.

15. Jansson KA, Linko E, Sandelin J, Harilainen A. A prospective randomized study of patellar versus hamstring tendon autografts for anterior cruciate ligament reconstruction. Am J Sports Med 2003;31(1):12-18.

16. Beynnon BD, Johnson RJ, Abate JA, Fleming BC, Nichols CE. Treatment of anterior cruciate ligament injuries, part 2. American Journal of Sports Medicine 2005;33(11):1751-1767.

17. Webster KE, Feller JA, Hameister KA. Bone tunnel enlargement following anterior cruciate ligament reconstruction: a randomised comparison of hamstring and patellar tendon grafts with 2-year follow-up. Knee Surgery Sports Traumatology Arthroscopy 2001;9(2):86-91.

18. Kousa P, Jarvinen TLN, Vihavainen M, Kannus P, Jarvinen M. The fixation strength of six hamstring tendon graft fixation devices in anterior cruciate ligament reconstruction - Part I: Femoral site. American Journal of Sports Medicine 2003;31(2):174-181.

19. Aglietti P, Buzzi R, Giron F, Simeone AJ, Zaccherotti G. Arthroscopic-assisted anterior cruciate ligament reconstruction with the central third patellar tendon. A 5-8-year follow-up. Knee Surg Sports Traumatol Arthrosc 1997;5(3):138-144.

20. Kullmer K, Letsch R, Turowski B. Which factors influence the progression of degenerative osteoarthritis after ACL surgery? Knee Surg Sports Traumatol Arthrosc 1994;2(2):80-84.

21. Sun Y, Sturmer T, Gunther KP, Brenner H. [Incidence and prevalence of cox- and gonarthrosis in the general population]. Z Orthop Ihre Grenzgeb 1997;135(3):184-92.

22. DeFrances CJ HM. 2002 National Hospital Discharge Survey: Advance Data from Vital Health Statistics. Report nr 342. Hyattsville, Maryland: National Center for Health Statistics; 2004.

23. Sharkey PF, Hozack WJ, Rothman RH, Shastri S, Jacoby SM. Why are total knee arthroplasties failing today? Clinical Orthopaedics and Related Research 2002; 404:7-13.

24. Harvey A, Thomas NP, Amis AA. Fixation of the graft in reconstruction of the anterior cruciate ligament. Journal of Bone and Joint Surgery-British Volume 2005;87B(5):593-603.

25. Arnold MR, Lie DTT, Verdonschot N, de Graaf R, Amis AA, van Kampen A. The remains of anterior cruciate ligament graft tension after cyclic knee motion. American Journal of Sports Medicine 2005;33(4):536-542.

26. Huang CH, Ma HM, Lee YM, Ho FY. Long-term results of low contact stress mobile-bearing total knee replacements. Clinical Orthopaedics and Related Research 2003;416:265-270.

27. Font-Rodriguez DE, Scuderi GR, Insall JN. Survivorship of cemented total knee arthroplasty. Clin Orthop Relat Res 1997;345:79-86.

28. Tissakht M, Ahmed AM, Chan KC. Calculated stress-shielding in the distal femur after total knee replacement corresponds to the reported location of bone loss. J Orthop Res 1996;14(5):778-785.

29. Savarino L, Tigani D, Greco M, Baldini N, Giunti A. The potential role of metal ion release as a marker of loosening in patients with total knee replacement A COHORT STUDY. Journal of Bone and Joint Surgery-British Volume 2010;92B(5):634-638.

30. Wakitani S, Goto T, Young RG, Mansour JM, Goldberg VM, Caplan AI. Repair of large full-thickness articular cartilage defects with allograft articular chondrocytes embedded in a collagen gel. Tissue Engineering 1998;4(4):429-444.

31. Brittberg M, Lindahl A, Nilsson A, Ohlsson C, Isaksson O, Peterson L. Treatment of deep cartilage defects in the knee with autologous chondrocyte transplantation. New England Journal of Medicine 1994;331(14):889-895.

32. Gillogly SD, Voight M, Blackburn T. Treatment of articular cartilage defects of the knee with autologous chondrocyte implantation. Journal of Orthopaedic & Sports Physical Therapy 1998;28(4):241-251.

33. Johnstone B, Hering TM, Caplan AI, Goldberg VM, Yoo JU. In vitro chondrogenesis of bone marrow-derived mesenchymal progenitor cells. Experimental Cell Research 1998;238(1):265-272.

34. Levin A, Burton-Wurster N, Chen CT, Lust G. Intercellular signaling as a cause of cell death in cyclically impacted cartilage explants. Osteoarthritis and Cartilage 2001;9(8):702-711.

35. Langer R, Vacanti JP. Tissue engineering. Science 1993;260(5110):920-926.

36. Griffith LG, Naughton G. Tissue engineering--current challenges and expanding opportunities. Science 2002;295(5557):1009-1014.

37. Ellis DL, Yannas IV. Recent advances in tissue synthesis in vivo by use of collagen-glycosaminoglycan copolymers. Biomaterials 1996;17(3):291-299.

38. Prockop DJ. Marrow stromal cells as steam cells for nonhematopoietic tissues. Science 1997;276(5309):71-74.

39. Bunnell BA, Flaat M, Gagliardi C, Patel B, Ripoll C. Adipose-derived stem cells: isolation, expansion and differentiation. Methods 2008;45(2):115-120.

40. Tavian M, Zheng B, Oberlin E, Crisan M, Sun B, Huard J, Peault B. The vascular wall as a source of stem cells. Hematopoietic Stem Cells V 2005;1044:41-50.

41. Caplan AI. Adult mesenchymal stem cells for tissue engineering versus regenerative medicine. Journal of Cellular Physiology 2007;213(2):341-347.

42. Martins-Green M, Hanafusa H. The 9E3/CEF4 gene and its product the chicken chemotactic and angiogenic factor (cCAF): potential roles in wound healing and tumor development. Cytokine Growth Factor Rev 1997;8(3):221-232.

43. Agrawal CM, Ray RB. Biodegradable polymeric scaffolds for musculoskeletal tissue engineering. J Biomed Mater Res 2001;55(2):141-150.

44. Kurtz S, Ong K, Lau E, Mowat F, Halpern M. Projections of primary and revision hip and knee arthroplasty in the United States from 2005 to 2030. Journal of Bone and Joint Surgery-American Volume 2007;89A(4):780-785.

45. Kurtz SM, Lau E, Ong K, Zhao K, Kelly M, Bozic KJ. Future young patient demand for primary and revision joint replacement: National Projections from 2010 to 2030. Clinical Orthopaedics and Related Research 2009;467(10):2606-2612.

46. Pelton AR, Stockel D, Duerig TW. Medical uses of nitinol. Shape Memory Materials 2000;327(3):63-70.

47. Polenichkin V, Pakhomenko G, Gyunter V, Khachin V, Itin V, Dudarev E.; Device for the fixation of bone fregments, Author's Certificate 850067, Inventions and Discoveries, USSR, November 1979.

48. Gil FJ, Planell JA. Effect of copper addition on the superelastic behavior of Ni-Ti shape memory alloys for orthodontic applications. Journal of Biomedical Materials Research 1999;48(5):682-688.

49. Gil FX, Manero JM, Planell JA. Relevant aspects in the clinical applications of NiTi shape memory alloys. Journal of Materials Science-Materials in Medicine 1996;7(7):403-406.

50. Wever DJ, Veldhuizen AG, Sanders MM, Schakenraad JM, vanHorn JR. Cytotoxic, allergic and genotoxic activity of a nickel-titanium alloy. Biomaterials 1997;18(16):1115-1120.

51. Ryhanen J, Kallioinen M, Tuukkanen J, Lehenkari P, Junila J, Niemela E, Sandvik P, Serlo W. Bone modeling and cell-material interface responses induced by nickel-titanium shape memory alloy after periosteal implantation. Biomaterials 1999;20(14):1309-1317.

52. Wever DJ, Veldhuizen AG, de Vries J, Busscher HJ, Uges DRA, van Horn JR. Electrochemical and surface characterization of a nickel-titanium alloy. Biomaterials 1998;19(7-9):761-769.

53. Duda SH, Pusich B, Richter G, Landwehr P, Oliva VL, Tielbeek A, Wiesinger B, Hak JB, Tielemans H, Ziemer G and others. Sirolimus-eluting stents for the treatment of obstructive superficial femoral artery disease. Circulation 2002;106(12):1505-1509.

54. Nakanishi T, Kondoh C, Nishikawa T, Satomi G, Nakazawa M, Imai Y, Momma K. Intravascular stents for management of pulmonary-artery and right-ventricular outflow obstruction. Heart and Vessels 1994;9(1):40-48.

55. Knirsch W, Haas NA, Lewin MA, Uhlemann F. Longitudinal stent fracture 11 months after implantation in the left pulmonary artery and successful

management by a stent-in-stent maneuver. Catheter Cardiovasc Interv 2003;58(1):116-118.

56. Shabalovskaya SA. Surface, corrosion and biocompatibility aspects of Nitinol as an implant material. Bio-Medical Materials and Engineering 2002;12(1):69-109.

57. Putters JL, Kaulesar Sukul DM, de Zeeuw GR, Bijma A, Besselink PA. Comparative cell culture effects of shape memory metal (Nitinol), nickel and titanium: A biocompatibility estimation. Eur Surg Res 1992;24(6):378-382.

58. Laing PG, Ferguson AB, Jr., Hodge ES. Tissue reaction in rabbit muscle exposed to metallic implants. J Biomed Mater Res 1967;1(1):135-149.

59. Wataha JC, O'Dell NL, Singh BB, Ghazi M, Whitford GM, Lockwood PE. Relating nickel-induced tissue inflammation to nickel release in vivo. J Biomed Mater Res 2001;58(5):537-544.

60. Coogan TP, Latta DM, Snow ET, Costa M. Toxicity and carcinogenicity of nickel compounds. Crc Critical Reviews in Toxicology 1989;19(4):341-384.

61. Hartwig A, Kruger I, Beyersmann D. Mechanisms in nickel genotoxicity - the significance of interactions with DNA-Repair. Toxicology Letters 1994;72(1-3):353-358.

62. Takahashi S, Takeda E, Kubota YH, Okayasu R. Inhibition of repair of radiation-induced DNA double-strand breaks by nickel and arsenite. Radiation Research 2000;154(6):686-691.

63. Peltonen L. Nickel sensitivity in the general population. Contact Dermatitis 1979;5(1):27-32.

64. Hildebrand HF, Veron C, Martin P. Nickel, chromium, cobalt dental alloys and allergic reactions - an overview. Biomaterials 1989;10(8):545-548.

65. Shabalovskaya SA. Physicochemical and biological aspects of Nitinol as a biomaterial. International Materials Reviews 2001;46(5):233-250.

66. Ryhanen J. Biocompatibility of nitinol. Minimally Invasive Therapy & Allied Technologies 2000;9(2):99-105.

67. Castleman LS, Motzkin SM, Alicandri FP, Bonawit VL, Johnson AA. Biocompatibility of nitinol alloy as an implant material. Journal of Biomedical Materials Research 1976;10(5):695-731.

68. Es-Souni M, Es-Souni M, Fischer-Brandies H. Assessing the biocompatibility of NiTi shape memory alloys used for medical applications. Analytical and Bioanalytical Chemistry 2005;381(3):557-567.

69. Hassel AW. Surface treatment of NiTi for medical applications. Minimally Invasive Therapy & Allied Technologies 2004;13(4):240-247.

70. Shevchenko N, Pham MT, Maitz MF. Studies of surface modified NiTi alloy. Applied Surface Science 2004;235(1-2):126-131.

71. Shih CC, Shih CM, Chen YL, Su YY, Shih JS, Kwok CF, Lin SJ. Growth inhibition of cultured smooth muscle cells by corrosion products of 316 L stainless steel wire. Journal of Biomedical Materials Research 2001;57(2):200-207.

72. Wataha JC, Lockwood PE, Marek M, Ghazi M. Ability of Ni-containing biomedical alloys to activate monocytes and endothelial cells in vitro. Journal of Biomedical Materials Research 1999;45(3):251-257.

73. Shih CC, Lin SJ, Chen YL, Su YY, Lai ST, Wu GJ, Kwok CF, Chung KH. The cytotoxicity of corrosion products of nitinol stent wire on cultured smooth muscle cells. Journal of Biomedical Materials Research 2000;52(2):395-403.

74. Heintz C, Riepe G, Birken L, Kaiser E, Chakfe N, Morlock M, Delling G, Imig H. Corroded nitinol wires in explanted aortic endografts: An important mechanism of failure? Journal of Endovascular Therapy 2001;8(3):248-253.

75. Jacobs TS, Won J, Gravereaux EC, Faries PL, Morrissey N, Teodorescu VJ, Hollier LH, Marin ML. Mechanical failure of prosthetic human implants: A 10-year experience with aortic stent graft devices. J Vasc Surg 2003;37(1):16-26.

76. Palmaz JC, Bailey S, Marton D, Sprague E. Influence of stent design and material composition on procedure outcome. J Vasc Surg 2002;36(5):1031-1039.

77. Riepe G, Heintz C, Kaiser E, Chakfe N, Morlock M, Delling M, Imig H. What can we learn from explanted endovascular devices? European Journal of Vascular and Endovascular Surgery 2002;24(2):117-122.

78. Metikos-Hukovic M, Kwokal A, Piljac J. The influence of niobium and vanadium on passivity of titanium-based implants in physiological solution. Biomaterials 2003;24(21):3765-3775.

79. Poggie RA, Kovacs P, Davidson JA. Oxygen diffusion hardening of Ti-Nb-Zr alloys. Materials and Manufacturing Processes 1996;11(2):185-197.

80. Godley R, Starosvetsky D, Gotman I. Corrosion behavior of a low modulus beta-Ti-45%Nb alloy for use in medical implants. Journal of Materials Science-Materials in Medicine 2006;17(1):63-67.

81. Lee CM, Ju CP, Lin JHC. Structure-property relationship of cast Ti-Nb alloys. Journal of Oral Rehabilitation 2002;29(4):314-322.

82. Kim HY, Ikehara Y, Kim JI, Hosoda H, Miyazaki S. Martensitic transformation, shape memory effect and superelasticity of Ti-Nb binary alloys. Acta Materialia 2006;54(9):2419-2429.

83. Kikuchi M, Takahashi M, Okuno O. Mechanical properties and grindability of dental cast Ti-Nb alloys. Dental Materials Journal 2003;22(3):328-342.

84. Kim HY, Satoru H, Kim JI, Hosoda H, Miyazaki S. Mechanical properties and shape memory behavior of Ti-Nb alloys. Materials Transactions 2004;45(7):2443-2448.

85. Kim JI, Kim HY, Inamura T, Hosoda H, Miyazaki S. Shape memory characteristics of Ti-22Nb-(2-8)Zr(at.%) biomedical alloys. Materials Science and Engineering a-Structural Materials Properties Microstructure and Processing 2005;403(1-2):334-339.

86. Liu R, Li DY. A finite element model study on wear resistance of pseudoelastic TiNi alloy. Materials Science and Engineering a-Structural Materials Properties Microstructure and Processing 2000;277(1-2):169-175.

87. Matsumoto H, Watanabe S, Hanada S. Beta TiNbSn alloys with low Young's modulus and high strength. Materials Transactions 2005;46(5):1070-1078.

88. Kujala S, Ryhanen J, Danilov A, Tuukkanen J. Effect of porosity on the osteointegration and bone ingrowth of a weight-bearing nickel-titanium bone graft substitute. Biomaterials 2003;24(25):4691-4697.

89. Wang XJ, Li YC, Xiong JY, Hodgson PD, Wen CE. Porous TiNbZr alloy scaffolds for biomedical applications. Acta Biomaterialia 2009;5(9):3616-3624.

90. Li JP, de Wijn JR, Van Blitterswijk CA, de Groot K. Porous Ti6Al4V scaffold directly fabricating by rapid prototyping: preparation and in vitro experiment. Biomaterials 2006;27(8):1223-1235.

91. Johnson CP, How T, Scraggs M, West CR, Burns J. A biomechanical study of the human vertebral artery with implications for fatal arterial injury. Forensic Science International 2000;109(3):169-182.

92. Hahn MS, McHale MK, Wang E, Schmedlen RH, West JL. Physiologic pulsatile flow bioreactor conditioning of poly(ethylene glycol)-based tissue engineered vascular grafts. Annals of Biomedical Engineering 2007;35(2):190-200.

93. Gregory TR. Nucleotypic effects without nuclei: Genome size and erythrocyte size in mammals. Genome 2000;43(5):895-901.

94. Wang YB, Zheng YF. Corrosion behaviour and biocompatibility evaluation of low modulus Ti-16Nb shape memory alloy as potential biomaterial. Materials Letters 2009;63(15):1293-1295.

95. El Medawar L, Rocher P, Hornez JC, Traisnel M, Breme J, Hildebrand HF. Electrochemical and cytocompatibility assessment of NiTiNOL memory shape alloy for orthodontic use. Biomolecular Engineering 2002;19(2-6):153-160.

96. Bogdanski D, Koller M, Muller D, Muhr G, Bram M, Buchkremer HP, Stover D, Choi J, Epple M. Easy assessment of the biocompatibility of Ni-Ti alloys by in vitro cell culture experiments on a functionally graded Ni-NiTi-Ti material. Biomaterials 2002;23(23):4549-4555.

97. Yeung KWK, Poon RWY, Chu PK, Chung CY, Liu XY, Lu WW, Chan D, Chan SCW, Luk KDK, Cheung KMC. Surface mechanical properties, corrosion resistance, and cytocompatibility of nitrogen plasma-implanted nickel-titanium alloys: A comparative study with commonly used medical grade materials. Journal of Biomedical Materials Research Part A 2007;82A(2):403-414.

98. Es-Souni M, Fischer-Brandies H. Human gingival fibroblast response to electropolished NiTi surfaces. J Biomed Mater Res A 2007;80(1):159-166.

99. Shabalovskaya SA, Rondelli GC, Undisz AL, Anderegg JW, Burleigh TD, Rettenmayr ME. The electrochemical characteristics of native Nitinol surfaces. Biomaterials 2009;30(22):3662-3671.

100. Undisz A, Schrempel F, Wesch W, Rettenmayr M. In situ observation of surface oxide layers on medical grade Ni-Ti alloy during straining. Journal of Biomedical Materials Research Part A 2009;88A(4):1000-1009.

101. Rondelli G, Vicentini B, Gigada A. The corrosion behavior of nickel titanium shape memory alloys. Corrosion Science 1990;30(8-9):805-812.

102. Hench L, Ethridge, EC. Biomaterials-the interfacial problem. Adv Biomed Eng 1975;5:35-150.

103. Watarai M, Hanawa T, Moriyama K, Asaoka K. Amount of metallic ions released from Ti-Ni alloy by abrasion in simulated bioliquids. Bio-Medical Materials and Engineering 1999;9(2):73-79.

104. Petrigliano FA, McAllister DR, Wu BM. Tissue engineering for anterior cruciate ligament reconstruction: A review of current strategies. Arthroscopy-the Journal of Arthroscopic and Related Surgery 2006;22(4):441-451.

105. Ge ZG, Yang F, Goh JCH, Ramakrishna S, Lee EH. Biomaterials and scaffolds for ligament tissue engineering. Journal of Biomedical Materials Research Part A 2006;77A(3):639-652.

106. Murray MM, Spindler KP. Anterior cruciate ligament healing and repair. Sports Medicine and Arthroscopy Review 2005;13(3):151-155.

107. Blackburn TA, Craig E. Knee anatomy: A brief review. Phys Ther 1980;60(12):1556-1560.

108. Brand J, Weiler A, Caborn DNM, Brown CH, Johnson DL. Graft fixation in cruciate ligament reconstruction. American Journal of Sports Medicine 2000;28(5):761-774.

109. Zhao JZ, Peng XC, He YH, Wang HH. Two-bundle anterior cruciate ligament reconstruction with eight-stranded hamstring tendons: Four-tunnel technique. Knee 2006;13(1):36-41.

110. Goldblatt JP, Fitzsimmons SE, Balk E, Richmond JC. Reconstruction of the anterior cruciate ligament: Meta-analysis of patellar tendon versus hamstring tendon autograft. Arthroscopy-the Journal of Arthroscopic and Related Surgery 2005;21(7):791-803.

111. Rose T, Engel T, Bernhard J, Hepp P, Josten C, Lill H. Differences in the rehabilitation period following two methods of anterior cruciate ligament replacement: Semitendinosus/gracilis tendon vs. ligamentum patellae. Knee Surgery Sports Traumatology Arthroscopy 2004;12(3):189-193.

112. Rahaman MN, Mao JJ. Stem cell-based composite tissue constructs for regenerative medicine. Biotechnology and Bioengineering 2005;91(3):261-284.

113. Vunjak-Novakovic G, Altman G, Horan R, Kaplan DL. Tissue engineering of ligaments. Annual Review of Biomedical Engineering 2004;6:131-156.

114. Jackson DW, Windler GE, Simon TM. Intraarticular reaction associated with the use of freeze-dried, ethylene oxide-sterilized bone-patella tendon-bone allografts

in the reconstruction of the anterior cruciate ligament. American Journal of Sports Medicine 1990;18(1):1-11.

115. Doroski DM, Brink KS, Temenoff JS. Techniques for biological characterization of tissue-engineered tendon and ligament. Biomaterials 2007;28(2):187-202.

116. Guidoin MF, Marois Y, Bejui J, Poddevin N, King MW, Guidoin R. Analysis of retrieved polymer fiber based replacements for the ACL. Biomaterials 2000;21(23):2461-2474.

117. Altman GH, Horan RL, Lu HH, Moreau J, Martin I, Richmond JC, Kaplan DL. Silk matrix for tissue engineered anterior cruciate ligaments. Biomaterials 2002;23(20):4131-4141.

118. Lu HH, Cooper JA, Manuel S, Freeman JW, Attawia MA, Ko FK, Laurencin CT. Anterior cruciate ligament regeneration using braided biodegradable scaffolds: In vitro optimization studies. Biomaterials 2005;26(23):4805-4816.

119. Freeman JW, Woods MD, Laurencin CT. Tissue engineering of the anterior cruciate ligament using a braid-twist scaffold design. Journal of Biomechanics 2007;40(9):2029-2036.

120. Wang JHC. Mechanobiology of tendon. Journal of Biomechanics 2006;39(9):1563-1582.

121. Pioletti DP, Rakotomanana LR, Leyvraz PF. Strain rate effect on the mechanical behavior of the anterior cruciate ligament-bone complex. Medical Engineering & Physics 1999;21(2):95-100.

122. Wang JHC, Thampatty BP, Lin JS, Im HJ. Mechanoregulation of gene expression in fibroblasts. Gene 2007;391(1-2):1-15.

123. Ma ZW, Kotaki M, Inai R, Ramakrishna S. Potential of nanofiber matrix as tissue-engineering scaffolds. Tissue Engineering 2005;11(1-2):101-109.

124. Riboldi SA, Sampaolesi M, Neuenschwander P, Cossu G, Mantero S. Electrospun degradable polyesterurethane membranes: Potential scaffolds for skeletal muscle tissue engineering. Biomaterials 2005;26(22):4606-4615.

125. Fong H, Chun I, Reneker DH. Beaded nanofibers formed during electrospinning. Polymer 1999;40(16):4585-4592.

126. Gupta P, Elkins C, Long TE, Wilkes GL. Electrospinning of linear homopolymers of poly(methyl methacrylate): exploring relationships between

fiber formation, viscosity, molecular weight and concentration in a good solvent. Polymer 2005;46(13):4799-4810.

127. Inoguchi H, Kwon IK, Inoue E, Takamizawa K, Maehara Y, Matsuda T. Mechanical responses of a compliant electrospun poly(L-lactide-co-epsilon-caprolactone) small-diameter vascular graft. Biomaterials 2006;27(8):1470-1478.

128. Nair LS, Bhattacharyya S, Bender JD, Greish YE, Brown PW, Allcock HR, Laurencin CT. Fabrication and optimization of methylphenoxy substituted polyphosphazene nanofibers for biomedical applications. Biomacromolecules 2004;5(6):2212-2220.

129. Engelmayr GC, Papworth GD, Watkins SC, Mayer JE, Sacks MS. Guidance of engineered tissue collagen orientation by large-scale scaffold microstructures. Journal of Biomechanics 2006;39(10):1819-1831.

130. Glass-Brudzinski JT, Perizzolo D, Brunette DM. Effects of substratum surface topography on the organization of cells and collagen fibers in collagen gel cultures. Journal of Biomedical Materials Research 2002;61(4):608-618.

131. Wang JHC, Jia FY, Gilbert TW, Woo SLY. Cell orientation determines the alignment of cell-produced collagenous matrix. Journal of Biomechanics 2003;36(1):97-102.

132. Frank C, Woo SLY, Amiel D, Harwood F, Gomez M, Akeson W. Medial collateral ligament healing - a multidisciplinary assessment in rabbits. American Journal of Sports Medicine 1983;11(6):379-389.

133. Kwon IK, Kidoaki S, Matsuda T. Electrospun nano- to microfiber fabrics made of biodegradable copolyesters: Structural characteristics, mechanical properties and cell adhesion potential. Biomaterials 2005;26(18):3929-3939.

134. Stankus JJ, Guan JJ, Wagner WR. Fabrication of biodegradable elastomeric scaffolds with sub-micron morphologies. Journal of Biomedical Materials Research Part A 2004;70A(4):603-614.

135. Xu CY, Inai R, Kotaki M, Ramakrishna S. Aligned biodegradable nanofibrous structure: A potential scaffold for blood vessel engineering. Biomaterials 2004;25(5):877-886.

136. Li MY, Mondrinos MJ, Gandhi MR, Ko FK, Weiss AS, Lelkes PI. Electrospun protein fibers as matrices for tissue engineering. Biomaterials 2005;26(30):5999-6008.

137. Bulick AS, Munoz-Pinto DJ, Qu X, Mani M, Cristancho D, Urban M, Hahn MS. Impact of Endothelial cells and mechanical conditioning on smooth muscle cell extracellular matrix production and differentiation. Tissue Engineering Part A 2009;15(4):815-825.

138. Guelcher SA, Srinivasan A, Dumas JE, Didier JE, McBride S, Hollinger JO. Synthesis, mechanical properties, biocompatibility, and biodegradation of polyurethane networks from lysine polyisocyanates. Biomaterials 2008;29(12):1762-1775.

139. Guelcher SA. Biodegradable polyurethanes: Synthesis and applications in regenerative medicine. Tissue Eng Part B Rev 2008;14(1):3-17.

140. Kavlock KD, Pechar TW, Hollinger JO, Guelcher SA, Goldstein AS. Synthesis and characterization of segmented poly(esterurethane urea) elastomers for bone tissue engineering. Acta Biomaterialia 2007;3(4):475-484.

141. Guelcher SA, Gallagher KM, Didier JE, Klinedinst DB, Doctor JS, Goldstein AS, Wilkes GL, Beckman EJ, Hollinger JO. Synthesis of biocompatible segmented polyurethanes from aliphatic diisocyanates and diurea diol chain extenders. Acta Biomater 2005;1(4):471-484.

142. Scotti C, Pozzi A, Mangiavini L, Vitari F, Boschetti F, Domeneghini C, Fraschini G, Peretti GM. Healing of meniscal tissue by cellular fibrin glue: An in vivo study. Knee Surgery Sports Traumatology Arthroscopy 2009;17(6):645-651.

143. Long JL, Tranquillo RT. Elastic fiber production in cardiovascular tissue-equivalents. Matrix Biology 2003;22(4):339-350.

144. Liu H, Collins SF, Suggs LJ. Three-dimensional culture for expansion and differentiation of mouse embryonic stem cells. Biomaterials 2006;27(36):6004-6014.

145. Hillwest JL, Chowdhury SM, Slepian MJ, Hubbell JA. Inhibition of thrombosis and intimal thickening by in-situ photopolymerization of thin hydrogel barriers. Proceedings of the National Academy of Sciences of the United States of America 1994;91(13):5967-5971.

146. Fung YC. Biomechanics: Mechanical Properties of Living Tissues. New York: Springer-Verlag; 1993.

147. Hirschi KK, Lai LH, Belaguli NS, Dean DA, Schwartz RJ, Zimmer WE. Transforming growth factor-beta induction of smooth muscle cell phenotpye

requires transcriptional and post-transcriptional control of serum response factor. Journal of Biological Chemistry 2002;277(8):6287-6295.

148. Isenberg BC, Tranquillo RT. Long-term cyclic distention enhances the mechanical properties of collagen-based media-equivalents. Annals of Biomedical Engineering 2003;31(8):937-949.

149. Bashur CA, Shaffer RD, Dahlgren LA, Guelcher SA, Goldstein AS. Effect of fiber diameter and alignment of electrospun polyurethane meshes on mesenchymal progenitor cells. Tissue Eng Part A 2009. 15:9, 2435-2445

150. Fisher NI. Statistical Analysis of Circular Data. Cambridge [England] ; New York, NY, USA: Cambridge University Press; 1993.

151. Syedain ZH, Weinberg JS, Tranquillo RT. Cyclic distension of fibrin-based tissue constructs: Evidence of adaptation during growth of engineered connective tissue. Proceedings of the National Academy of Sciences of the United States of America 2008;105(18):6537-6542.

152. Johnson C, Grant R, Dansie B, Taylor J, Spyropolous P. Measurement of blood flow in the vertebral artery using colour duplex Doppler ultrasound: Establishment of the reliability of selected parameters. Manual Therapy 2000;5(1):21-29.

153. Bryant SJ, Nuttelman CR, Anseth KS. Cytocompatibility of UV and visible light photoinitiating systems on cultured NIH/3T3 fibroblasts in vitro. Journal of Biomaterials Science-Polymer Edition 2000;11(5):439-457.

154. Kim BS, Nikolovski J, Bonadio J, Mooney DJ. Cyclic mechanical strain regulates the development of engineered smooth muscle tissue. Nature Biotechnology 1999;17(10):979-983.

155. Huang L, McMillan RA, Apkarian RP, Pourdeyhimi B, Conticello VP, Chaikof EL. Generation of synthetic elastin-mimetic small diameter fibers and fiber networks. Macromolecules 2000;33(8):2989-2997.

156. See EYS, Toh SL, Goh JCH. BMSC Sheets for ligament tissue engineering. 13th International Conference on Biomedical Engineering, 2009;23(1-3):1508-1511.

157. Li Y, Ma T, Kniss DA, Lasky LC, Yang ST. Effects of filtration seeding on cell density, spatial distribution, and proliferation in nonwoven fibrous matrices. Biotechnology Progress 2001;17(5):935-944.

158. Wendt D, Marsano A, Jakob M, Heberer M, Martin I. Oscillating perfusion of cell suspensions through three-dimensional scaffolds enhances cell seeding efficiency and uniformity. Biotechnology and Bioengineering 2003;84(2):205-214.

159. Kim BS, Putnam AJ, Kulik TJ, Mooney DJ. Optimizing seeding and culture methods to engineer smooth muscle tissue on biodegradable polymer matrices. Biotechnol Bioeng 1998;57(1):46-54.

160. Canavan HE, Cheng XH, Graham DJ, Ratner BD, Castner DG. Cell sheet detachment affects the extracellular matrix: A surface science study comparing thermal liftoff, enzymatic, and mechanical methods. Journal of Biomedical Materials Research Part A 2005;75A(1):1-13.

161. Shimizu T, Yamato M, Kikuchi A, Okano T. Cell sheet engineering for myocardial tissue reconstruction. Biomaterials 2003;24(13):2309-2316.

162. L'Heureux N, Paquet S, Labbe R, Germain L, Auger FA. A completely biological tissue-engineered human blood vessel. FASEB J 1998;12(1):47-56.

163. Michel M, L'Heureux N, Pouliot R, Xu W, Auger FA, Germain L. Characterization of a new tissue-engineered human skin equivalent with hair. In Vitro Cellular & Developmental Biology-Animal 1999;35(6):318-326.

164. Ge ZG, Goh JCH, Lee EH. Selection of cell source for ligament tissue engineering. Cell Transplantation 2005;14(8):573-583.

165. Van Eijk F, Saris DB, Riesle J, Willems WJ, Van Blitterswijk CA, Verbout AJ, Dhert WJ. Tissue engineering of ligaments: A comparison of bone marrow stromal cells, anterior cruciate ligament, and skin fibroblasts as cell source. Tissue Eng 2004;10(5-6):893-903.

166. Altman GH, Horan RL, Martin I, Farhadi J, Stark PRH, Volloch V, Richmond JC, Vunjak-Novakovic G, Kaplan DL. Cell differentiation by mechanical stress. Faseb Journal 2001;15(14):270-278.

167. Curtis A, Riehle M. Tissue engineering: the biophysical background. Physics in Medicine and Biology 2001;46(4):R47-R65.

168. Flemming RG, Murphy CJ, Abrams GA, Goodman SL, Nealey PF. Effects of synthetic micro- and nano-structured surfaces on cell behavior. Biomaterials 1999;20(6):573-588.

169. Li D, Wang YL, Xia YN. Electrospinning of polymeric and ceramic nanofibers as uniaxially aligned arrays. Nano Letters 2003;3(8):1167-1171.

170. den Braber ET, de Ruijter JE, Ginsel LA, von Recum AF, Jansen JA. Orientation of ECM protein deposition, fibroblast cytoskeleton, and attachment complex components on silicone microgrooved surfaces. J Biomed Mater Res 1998;40(2):291-300.

171. den Braber ET, Jansen HV, de Boer MJ, Croes HJE, Elwenspoek M, Ginsel LA, Jansen JA. Scanning electron microscopic, transmission electron microscopic, and confocal laser scanning microscopic observation of fibroblasts cultured on microgrooved surfaces of bulk titanium substrata. Journal of Biomedical Materials Research 1998;40(3):425-433.

172. Walboomers XF, Ginsel LA, Jansen JA. Early spreading events of fibroblasts on microgrooved substrates. J Biomed Mater Res 2000;51(3):529-534.

173. Johansson F, Carlberg P, Danielsen N, Montelius L, Kanje M. Axonal outgrowth on nano-imprinted patterns. Biomaterials 2006;27(8):1251-1258.

174. Clark P, Connolly P, Curtis ASG, Dow JAT, Wilkinson CDW. Cell guidance by ultrafine topography in vitro. Journal of Cell Science 1991;99:73-77.

175. Lee CH, Shin HJ, Cho IH, Kang YM, Kim IA, Park KD, Shin JW. Nanofiber alignment and direction of mechanical strain affect the ECM production of human ACL fibroblast. Biomaterials 2005;26(11):1261-1270.

176. Bashur CA, Dahlgren LA, Goldstein AS. Effect of fiber diameter and orientation on fibroblast morphology and proliferation on electrospun poly(D,L-lactic-co-glycolic acid) meshes. Biomaterials 2006;27(33):5681-5688.

177. McMahon RE QX, XJimenez-Vergara AC, Bashur CA, Guelcher SA, Goldstein AS, Hahn MS. Electrospun mesh-hydrogel composites for tissue engineered vascular grafts. Tissue Engineering, in press.

178. Norton J, Barie PS, Bollinger RR, Chang AE, Pass HI, Thompson RW. Surgery: Basic Science and Clinical Evidence. New York, NY: Springer; 2008.

179. Nieponice A, Soletti L, Guan JJ, Deasy BM, Huard J, Wagner WR, Vorp DA. Development of a tissue-engineered vascular graft combining a biodegradable scaffold, muscle-derived stem cells and a rotational vacuum seeding technique. Biomaterials 2008;29(7):825-833.

180. Woo SLY, Hildebrand K, Watanabe N, Fenwick JA, Papageorgiou CD, Wang JHC. Tissue engineering of ligament and tendon healing. Clinical Orthopaedics and Related Research 1999(367):S312-S323.

181. Fu FH, Bennett CH, Lattermann C, Ma CB. Current trends in anterior cruciate ligament reconstruction part 1: Biology and biomechanics of reconstruction. American Journal of Sports Medicine 1999;27(6):821-830.

182. Weitzel PP, Richmond JC, Altman GH, Calabro T, Kaplan DL. Future direction of the treatment of ACL ruptures. Orthopedic Clinics of North America 2002;33(4):653-661.

183. Vunjak-Novakovic G, Altman G, Horan R, Kaplan DL. Tissue engineering of ligaments. Annu Rev Biomed Eng 2004;6:131-156.

184. Deehan DJ, Cawston TE. The biology of integration of the anterior cruciate ligament. Journal of Bone and Joint Surgery-British Volume 2005;87B(7):889-895.

185. Lu HH, Jiang J. Interface tissue engineering and the formulation of multiple-tissue systems. Tissue Engineering I: Scaffold Systems for Tissue Engineering 2006;102:91-111.

186. Friedman MJ, Sherman OH, Fox JM, Del Pizzo W, Snyder SJ, Ferkel RJ. Autogeneic anterior cruciate ligament (ACL) anterior reconstruction of the knee. A review. Clin Orthop Relat Res 1985(196):9-14.

187. Robertson DB, Daniel DM, Biden E. Soft tissue fixation to bone. Am J Sports Med 1986;14(5):398-403.

188. Thomopoulos S, Williams GR, Gimbel JA, Favata M, Soslowsky LJ. Variation of biomechanical, structural, and compositional properties along the tendon to bone insertion site. Journal of Orthopaedic Research 2003;21(3):413-419.

189. Yang PJ, Temenoff JS. Engineering orthopedic tissue interfaces. Tissue Engineering Part B-Reviews 2009;15(2):127-141.

190. Phillips JE, Burns KL, Le Doux JM, Guldberg RE, Garcia AJ. Engineering graded tissue interfaces. Proc Natl Acad Sci USA 2008;105(34):12170-12175.

191. Ducheyne P, Qiu Q. Bioactive ceramics: The effect of surface reactivity on bone formation and bone cell function. Biomaterials 1999;20(23-24):2287-2303.

192. Kretlow JD, Mikos AG. Review: Mineralization of synthetic polymer scaffolds for bone tissue engineering. Tissue Engineering 2007;13(5):927-938.

193. Garcia AJ, Ducheyne P, Boettiger D. Effect of surface reaction stage on fibronectin-mediated adhesion of osteoblast-like cells to bioactive glass. Journal of Biomedical Materials Research 1998;40(1):48-56.

194. Khan Y, Yaszemski MJ, Mikos AG, Laurencin CT. Tissue engineering of bone: Material and matrix considerations. Journal of Bone and Joint Surgery-American Volume 2008;90A:36-42.

195. Ning CQ, Mehta J, El-Ghannam A. Effects of silica on the bioactivity of calcium phosphate composites in vitro. Journal of Materials Science-Materials in Medicine 2005;16(4):355-360.

196. Gupta G, El-Ghannam A, Kirakodu S, Khraisheh M, Zbib H. Enhancement of osteoblast gene expression by mechanically compatible porous Si-rich nanocomposite. Journal of Biomedical Materials Research Part B-Applied Biomaterials 2007;81B(2):387-396.

197. Song JH, Yoon BH, Kim HE, Kim HW. Bioactive and degradable hybridized nanofibers of gelatin-siloxane for bone regeneration. Journal of Biomedical Materials Research Part A 2008;84A(4):875-884.

198. DeLong SA, Moon JJ, West JL. Covalently immobilized gradients of bFGF on hydrogel scaffolds for directed cell migration. Biomaterials 2005;26(16):3227-3234.

199. Hahn MS, Miller JS, West JL. Three-dimensional biochemical and biomechanical patterning of hydrogels for guiding cell behavior. Advanced Materials 2006;18(20):2679-2684.

200. Hahn MS, Taite LJ, Moon JJ, Rowland MC, Ruffino KA, West JL. Photolithographic patterning of polyethylene glycol hydrogels. Biomaterials 2006;27(12):2519-2524.

201. Miller JS, Bethencourt MI, Hahn M, Lee TR, West JL. Laser-scanning lithography (LSL) for the soft lithographic patterning of cell-adhesive self-assembled monolayers. Biotechnology and Bioengineering 2006;93(6):1060-1068.

202. McDonald JC, Whitesides GM. Poly(dimethylsiloxane) as a material for fabricating microfluidic devices. Accounts of Chemical Research 2002;35(7):491-499.

203. Gong CG, Frechet JMJ. End functionalization of hyperbranched poly(siloxysilane): Novel crosslinking agents and hyperbranched-linear star block copolymers. Journal of Polymer Science Part A-Polymer Chemistry 2000;38(16):2970-2978.

204. Panda DK, Miao DS, Lefebvre V, Hendy GN, Goltzman D. The transcription factor SOX9 regulates cell cycle and differentiation genes in chondrocytic CFK2 cells. Journal of Biological Chemistry 2001;276(44):41229-41236.

205. Grunlan MA, Lee NS, Mansfeld F, Kus E, Finlay JA, Callow JA, Callow ME, Weber WP. Minimally adhesive polymer surfaces prepared from star oligosiloxanes and star oligofluorosiloxanes. Journal of Polymer Science Part A-Polymer Chemistry 2006;44(8):2551-2566.

206. Murthy R, Shell CE, Grunlan MA. The influence of poly(ethylene oxide) grafting via siloxane tethers on protein adsorption. Biomaterials 2009;30(13):2433-2439.

207. Ducheyne P, Qiu Q. Bioactive ceramics: The effect of surface reactivity on bone formation and bone cell function. Biomaterials 1999;20(23-24):2287-2303.

208. El-Ghannam AR. Advanced bioceramic composite for bone tissue engineering: Design principles and structure-bioactivity relationship. Journal of Biomedical Materials Research Part A 2004;69A(3):490-501.

209. Ford MC, Bertram JP, Hynes SR, Michaud M, Li Q, Young M, Segal SS, Madri JA, Lavik EB. A macroporous hydrogel for the coculture of neural progenitor and endothelial cells to form functional vascular networks in vivo. Proceedings of the National Academy of Sciences of the United States of America 2006;103(8):2512-2517.

210. Canal T, Peppas NA. Correlation between mesh size and equilibrium degree of swelling of polymeric networks. Journal of Biomedical Materials Research 1989;23(10):1183-1193.

211. Mellott MB, Searcy K, Pishko MV. Release of protein from highly cross-linked hydrogels of poly(ethylene glycol) diacrylate fabricated by UV polymerization. Biomaterials 2001;22(9):929-941.

212. Watkins AW, Anseth KS. Investigation of molecular transport and distributions in poly(ethylene glycol) hydrogels with confocal laser scanning microscopy. Macromolecules 2005;38(4):1326-1334.

213. Anseth KS, Metters AT, Bryant SJ, Martens PJ, Elisseeff JH, Bowman CN. In situ forming degradable networks and their application in tissue engineering and drug delivery. Journal of Controlled Release 2002;78(1-3):199-209.

214. Liao H, Munoz-Pinto D, Qu X, Hou Y, Grunlan MA, Hahn MS. Influence of hydrogel mechanical properties and mesh size on vocal fold fibroblast extracellular matrix production and phenotype. Acta Biomater 2008;4(5):1161-71.

215. Miller EJ, Gay S. Collagen - an overview. Methods in Enzymology 1982;82:3-32.

216. Munoz-Pinto DJ, Bulick AS, Hahn MS. Uncoupled investigation of scaffold modulus and mesh size on smooth muscle cell behavior. Journal of Biomedical Materials Research Part A 2009;90A(1):303-316.

217. Salinas CN, Anseth KS. The influence of the RGD peptide motif and its contextual presentation in PEG gels on human mesenchymal stem cell viability. Journal of Tissue Engineering and Regenerative Medicine 2008;2(5):296-304.

218. Salinas CN, Anseth KS. The enhancement of chondrogenic differentiation of human mesenchymal stem cells by enzymatically regulated RGD functionalities. Biomaterials 2008;29(15):2370-2377.

219. Burdick JA, Anseth KS. Photoencapsulation of osteoblasts in injectable RGD-modified PEG hydrogels for bone tissue engineering. Biomaterials 2002;23(22):4315-4323.

220. Benoit DSW, Schwartz MP, Durney AR, Anseth KS. Small functional groups for controlled differentiation of hydrogel-encapsulated human mesenchymal stem cells. Nature Materials 2008;7(10):816-823.

221. Lim JY, Shaughnessy MC, Zhou ZY, Noh H, Vogler EA, Donahue HJ. Surface energy effects on osteoblast spatial growth and mineralization. Biomaterials 2008;29(12):1776-1784.

222. Murthy R, Cox CD, Hahn MS, Grunlan MA. Protein-resistant silicones: Incorporation of poly(ethylene oxide) via siloxane tethers. Biomacromolecules 2007;8(10):3244-3252.

223. Gombotz WR, Guanghui W, Horbett TA, Hoffman AS. Protein adsorption to poly(ethylene oxide) surfaces. Journal of Biomedical Materials Research 1991;25(12):1547-1562.

224. Peyton SR, Raub CB, Keschrumrus VP, Putnam AJ. The use of poly(ethylene glycol) hydrogels to investigate the impact of ECM chemistry and mechanics on smooth muscle cells. Biomaterials 2006;27(28):4881-4893.

225. Baker BM, Gee AO, Metter RB, Nathan AS, Marklein RA, Burdick JA, Mauck RL. The potential to improve cell infiltration in composite fiber-aligned electrospun scaffolds by the selective removal of sacrificial fibers. Biomaterials 2008;29(15):2348-2358.

226. Dalton PD, Klinkhammer K, Salber J, Klee D, Moller M. Direct in vitro electrospinning with polymer melts. Biomacromolecules 2006;7(3):686-690.

227. Munoz-Pinto DJ, McMahon RE, Kanzelberger MA, Jimenez-Vergara AC, Grunlan MA, Hahn MS. Inorganic-organic hybrid scaffolds for osteochondral regeneration. J Biomed Mater Res A;2010 94(1):112-121.

228. Engler AJ, Sen S, Sweeney HL, Discher DE. Matrix elasticity directs stem cell lineage specification. Cell 2006;126(4):677-689.

229. Dawson E, Mapili G, Erickson K, Taqvi S, Roy K. Biomaterials for stem cell differentiation. Adv Drug Deliv Rev 2008;60(2):215-228.

VITA

Name: Rebecca Erin McMahon

Address: 200 Jack E Brown Building
3122 TAMU
College Station, TX 77843-3122

Email Address: rebecca.erin.mcmahon@gmail.com

Education: B.S., Dual: Chemical Engineering and Science, Technology and Society, Rensselaer Polytechnic Institute, 2007

Publications: **R.E. McMahon***, X. Qu*, A.C. Jimenez-Vergara, C.A. Bashur, S.A. Guelcher, A.S. Goldstein, M.S. Hahn. Electrospun mesh-hydrogel composites for tissue engineered vascular grafts. Tissue Eng. C, in press.

D. Munoz-Pinto*, **R. McMahon***, M. Kanzelberger, A.C. Jimenez-Vergara, Y. Hou, M. Grunlan, *M.S. Hahn*. (2010). Inorganic-organic hybrid scaffolds for osteochondral regeneration. J of Biomed Mater Res A. 94 (1): 112-21. PMID: 20128006

C.A. Jimenez-Vergara, **R. McMahon**, D. Munoz-Pinto, L.Cubero-Ponce, A. Morales, *M.S. Hahn*. (2010). Approach for fabricating tissue engineered vascular grafts with stable endothelialization. Annals of Biomedical Engineering. 38 (9): 2885-95

X. Qu, AC Jimenez-Vergara, D.J. Munoz-Pinto, D. Ortiz, **R.E. McMahon**, D Cristancho, S. Becerra-Bayona, V. Guiza-Arguello, K.J. Grande-Allen, M.S. Hahn. Regulation of smooth muscle cell phenotype by glycosaminoglycan identity. Acta Biomaterialia, in press.

D. Munoz-Pinto, C.A. Jimenez-Vergara, L.M. Gelves, **R. McMahon**, V. Guiza-Arguello, *M.S. Hahn*. (2009). Probing vocal fold fibroblast response to hyaluronan in controlled 3D contexts. Biotechnology and Bioengineering. 104 (4): 821-31. PMID: 19718686

*Authors contributed equally to this work

Awards: Rensselaer Medal (2004)